Neuron
Article

State Dependence of Noise Correlations in Macaque Primary Visual Cortex

Alexander S. Ecker,[1,2,3,5,*] Philipp Berens,[1,2,3] R. James Cotton,[1] Manivannan Subramaniyan,[1] George H. Denfield,[1] Cathryn R. Cadwell,[1] Stelios M. Smirnakis,[1,4] Matthias Bethge,[2,3,5] and Andreas S. Tolias[1,3,6,*]
[1]Department of Neuroscience, Baylor College of Medicine, Houston, TX, USA
[2]Werner Reichardt Centre for Integrative Neuroscience and Institute of Theoretical Physics, University of Tübingen, Germany
[3]Bernstein Center for Computational Neuroscience, Tübingen, Germany
[4]Department of Neurology, Baylor College of Medicine, Houston, TX, USA
[5]Max Planck Institute for Biological Cybernetics, Tübingen, Germany
[6]Department of Computational and Applied Mathematics, Rice University, Houston, TX, USA
*Correspondence: alexander.ecker@uni-tuebingen.de (A.S.E.), astolias@bcm.edu (A.S.T.)
http://dx.doi.org/10.1016/j.neuron.2014.02.006

SUMMARY

Shared, trial-to-trial variability in neuronal populations has a strong impact on the accuracy of information processing in the brain. Estimates of the level of such noise correlations are diverse, ranging from 0.01 to 0.4, with little consensus on which factors account for these differences. Here we addressed one important factor that varied across studies, asking how anesthesia affects the population activity structure in macaque primary visual cortex. We found that under opioid anesthesia, activity was dominated by strong coordinated fluctuations on a timescale of 1–2 Hz, which were mostly absent in awake, fixating monkeys. Accounting for these global fluctuations markedly reduced correlations under anesthesia, matching those observed during wakefulness and reconciling earlier studies conducted under anesthesia and in awake animals. Our results show that internal signals, such as brain state transitions under anesthesia, can induce noise correlations but can also be estimated and accounted for based on neuronal population activity.

INTRODUCTION

A ubiquitous property of cortical neurons is their high degree of response variability (Softky and Koch, 1993). Since repeated presentations of the same stimulus never elicit the same response twice, an accurate representation of the stimulus can be obtained only by considering the joint response profile of populations of neurons. The accuracy of such a population code strongly depends on neuronal correlations (Averbeck et al., 2006; Zohary et al., 1994; Abbott and Dayan, 1999; Sompolinsky et al., 2001). Specifically, noise correlations, which express the amount of covariability in the trial-to-trial fluctuations of responses of two neurons to repeated presentations of the same stimulus, are central to such questions of coding accuracy.

In recent years, both the level and the origin of such noise correlations have been subject to debate. While it was originally suggested that noise correlations arise due to shared sensory noise arising in the afferent sensory pathway (Zohary et al., 1994; Shadlen and Newsome, 1998), more recent studies suggest that they in fact represent meaningful top-down signals generated internally to the brain (Cohen and Newsome, 2008; Nienborg and Cumming, 2009; Ecker et al., 2010). Moreover, the observed level of correlations varies greatly between studies, with average values ranging from 0.01 to 0.4 (Bach and Krüger, 1986; Zohary et al., 1994; Gawne and Richmond, 1993; Gawne et al., 1996; Bair et al., 2001; Kohn and Smith, 2005; Gutnisky and Dragoi, 2008; Smith and Kohn, 2008; Cohen and Newsome, 2008; Mitchell et al., 2009; Cohen and Maunsell, 2009; Ecker et al., 2010; Hansen et al., 2012; Smith et al., 2013; Smith and Sommer, 2013; Herrero et al., 2013). It has recently been suggested that much of the differences between studies may be accounted for by differences in firing rates (Cohen and Kohn, 2011). However, there are striking differences in correlations even between studies conducted in the same brain area with similar stimuli and similar firing rates (e.g., Smith and Kohn, 2008; Ecker et al., 2010), suggesting that the firing rate dependence is insufficient to explain the variability across studies and other factors need to be taken into account as well.

One such factor that varies across studies is anesthesia. It constitutes a drastic alteration of global brain state, the mechanisms of which are only partly understood and depend on drugs that are used (Campagna et al., 2003). One of the most striking features of anesthesia, also observed during natural deep sleep, are strong slow-wave oscillations in the electroencephalogram (EEG) at frequencies below 2 Hz (Steriade et al., 1993). Many commonly used anesthetics, such as isoflurane, urethane, and ketamine, substantially alter neural activity by suppressing sensory responses and increasing response latencies (Angel, 1993; Drummond, 2000; Chi and Field, 1986; Kohn et al., 2009) as well as inducing so-called up and down states (Renart et al., 2010; Constantinople and Bruno, 2011; Harris and Thiele, 2011). Some neuroscientists resort to opioids, such as fentanyl or sufentanil (Kohn and Smith, 2005; Smith and Kohn, 2008; Reich et al., 2001), which are believed to affect neural activity in less dramatic ways (Loughnan et al., 1987; Schwender et al., 1993;

Drummond, 2000; Constantinople and Bruno, 2011). However, although opioids seem to have a number of advantages over other drugs, they have similarly been shown to affect neural response properties (Schwender et al., 1993) and induce low-frequency oscillations (Bowdle and Ward, 1989).

To shed light on how opioids modify the structure of neural population activity, we measured noise correlations in primary visual cortex of anesthetized and awake monkeys using identical recording techniques. Under anesthesia we observed periods of almost complete silence across the population as well as periods of very strong activity. These periods lasted for a few hundred milliseconds, arose spontaneously, and were not linked to the visual stimulus. They resembled up and down states commonly observed using nonopioid anesthetics (Renart et al., 2010; Constantinople and Bruno, 2011; Harris and Thiele, 2011), and their characteristic frequency was comparable to slow-wave oscillations in the EEG (Steriade et al., 1993). Interestingly, they could be almost completely accounted for by a latent variable model of the population activity with a single latent variable indicating the network state. When we conditioned on this latent variable, the magnitude and structure of noise correlations under anesthesia were almost indistinguishable from those we observed previously in awake monkeys (Ecker et al., 2010).

Our results show that spontaneous transitions in network state under anesthesia induce noise correlations between neurons. These transitions are absent in awake, fixating monkeys. This indicates a clear qualitative difference between the two states despite similar firing rates. Thus, anesthesia is an important, but often neglected, factor accounting for differences between studies that cannot be explained by firing rates, as suggested previously (Cohen and Kohn, 2011).

RESULTS

First- and Second-Order Statistics of Neuronal Responses

We recorded the spiking activity of populations of neurons in primary visual cortex of awake and anesthetized macaque monkeys. We recorded from 487 neurons in two awake monkeys and 636 neurons in three anesthetized monkeys. Our data set consists of 58 recording sessions (31 awake and 27 anesthetized), each containing 10 to 42 simultaneously recorded cells (medians were 15 for awake and 23 for anesthetized recordings). The awake data set is a subset of previously published data (Ecker et al., 2010) (see Experimental Procedures for details). We presented sinusoidal gratings covering the receptive fields of all recorded neurons. Gratings were drifting, except in 14 of the awake sessions where static gratings were shown.

As expected, neurons in V1 of awake monkeys were robustly driven by the grating stimulus (Figure 1A), and the vast majority of cells were tuned to orientation (Figure 1B) (for this example session: 27/29 cells; overall 82% or 400/487 cells at $p < 0.01$; permutation test; not corrected for multiple testing). The same was true for anesthetized recordings (Figures 1C and 1D), where an even larger fraction of cells was tuned (example session: all 44 cells; overall 92% or 586/636 cells tuned at $p < 0.01$), probably reflecting the fact that anesthetized recordings on average contained larger amounts of data. Thus, when averaging spike trains across multiple trials, responses recorded during wakefulness and under anesthesia were qualitatively similar, in the sense that a large fraction of cells was robustly tuned to orientation.

We noticed, however, that anesthetized responses appeared noisier than those recorded during wakefulness (Figures 1A and 1C). To test whether this impression was true at the population level, we computed the Fano factors (variance of the response divided by its mean) for all recorded neurons. Indeed, response variability was roughly twice as large under anesthesia as during wakefulness (Figure 2A) (average $F = 2.2$ versus 1.2, respectively; $p < 10^{-15}$, Wilcoxon rank-sum test). This was not due to systematic differences in firing rates between wakefulness and anesthesia, as it was true for the entire range of firing rates (Figure 2B).

This increased trial-to-trial variability could be a single-neuron effect, where the anesthetic causes individual neurons to fire more randomly, or a population effect, where groups of neurons are comodulated by a common source present only under anesthesia. While the former would add independent noise and manifest itself primarily in increased variances (and Fano factors), the latter would also give rise to elevated noise correlations. Indeed, the average level of correlations was roughly six times higher under anesthesia than during wakefulness (Figure 2C) (0.05 versus 0.008, respectively; $p < 10^{-15}$, Wilcoxon rank-sum test; 8,012 versus 3,878 pairs). Again, this difference was present at the full range of firing rates and most prominent for pairs of cells with high rates (Figure 2D).

State Fluctuations under Anesthesia

Our data seem to argue for a population-level effect of anesthesia, where many neurons are modulated simultaneously on a trial-to-trial basis. Indeed, population raster plots showing the activity of all simultaneously recorded neurons for a given trial revealed periods of almost complete silence as well as periods of vigorous activity (Figure 3C) (see e.g., trials 2 through 4). The transitions between such periods seemed to arise spontaneously and were not linked to the stimulus, suggesting that at least part of the increased variability was caused by a common noise source.

To characterize this common source of variability in more detail, we used a recently developed latent variable model called Gaussian Process Factor Analysis (GPFA) (Figure 3A; Experimental Procedures for details) (Yu et al., 2009). The GPFA model promises to be a good candidate for capturing the phenomena observed here, as it seeks to describe the correlations in the data by a low-dimensional state variable, which evolves smoothly in time and affects each neuron's firing rate linearly. We use the GPFA model to represent the fluctuations around the stimulus-driven response (noise correlations):

$$y_k(t) = f_k(s(t)) + c_k x(t) + \eta. \quad (1)$$

Here, $f_k(s(t))$ is the time-resolved tuning curve of neuron k, which captures the stimulus-induced response dynamics; $x(t)$ is the network state, which is a one-dimensional function of time; c_k is the weight that determines how x affects the neuron's response; and η is independent Gaussian noise. The network state x has a smooth autocorrelation function with timescale τ (Figure 3A; Experimental Procedures).

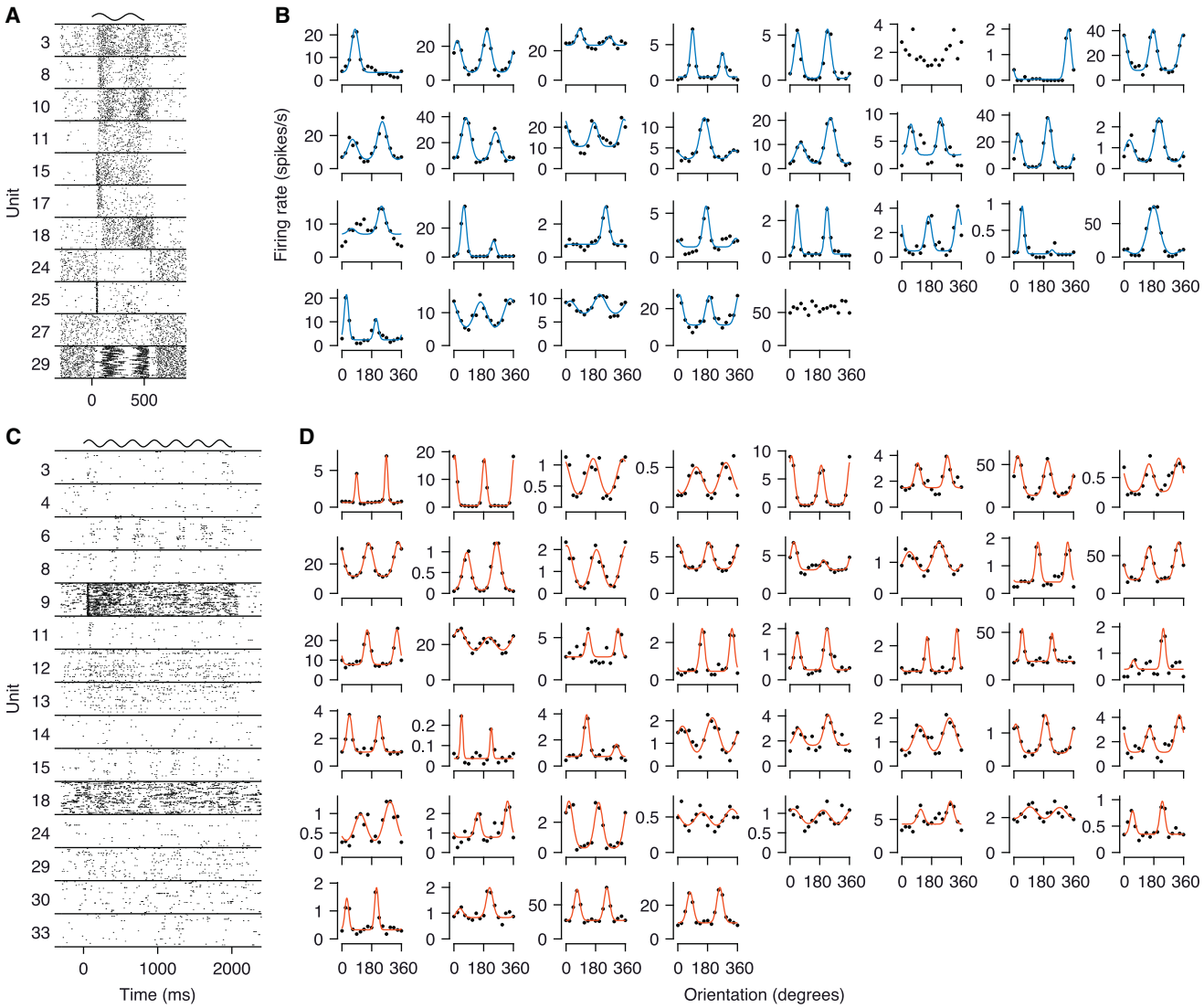

Figure 1. Recordings of Population Activity in V1

(A) Spike rasters for a subset of the neurons recorded in one example session during wakefulness. The sinusoid at the top indicates the stimulus duration (500 ms) and its temporal frequency. Numbers, neuron numbers in (B), counted from left to right, top to bottom.

(B) Tuning curves for all neurons in the same session as in (A). Solid lines show least-squares fit, shown only for cells significantly tuned to orientation (27/29 cells at $p < 0.01$; noncorrected).

(C) Spike rasters during anesthesia, as in (A).

(D) Tuning curves, as in (B); all 44 neurons significantly tuned at $p < 0.001$.

Using such a latent variable model affords several advantages over the traditional approach of computing pairwise correlations and analyzing their relationship to other quantities such as signal correlations or distance between neurons. First, the number of parameters that need to be estimated is substantially lower than when estimating the full correlation matrix. Second, if there are processes contributing to the observed correlations that affect many neurons at the same time, they can be estimated more efficiently, and their timescale can be extracted simultaneously.

The GPFA model with a single state variable captured the structure and dynamics of the population response under anesthesia well. Visually, the estimate of the network state corresponded well to the apparent on and off periods (Figure 3C). We quantified how much explanatory power the network state variable has under the two different brain states by computing the fraction of variance explained (VE) (see Experimental Procedures for details) on a separate subset of the data not used for fitting the model. In the awake data set, the state variable explained on average less than 5% of the variance (Figures 3D–3F). Strikingly, under anesthesia, up to 40% of individual cells' variances were explained by network state (Figures 3E and 3F). To ensure that this effect was not due to longer trials in our anesthetized experiments (2 s anesthetized versus 500 ms

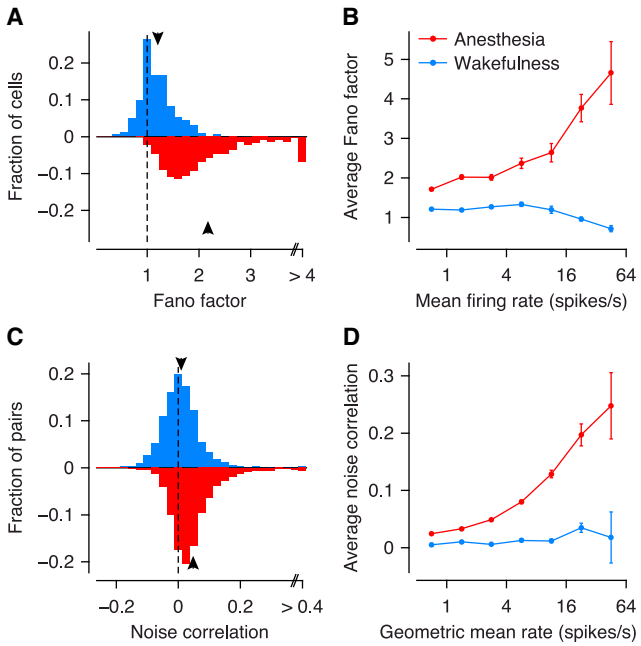

Figure 2. Fano Factors and Noise Correlations during Wakefulness (Blue) and Anesthesia (Red)

(A) Distribution of Fano factors. Arrows indicate means.

(B) Dependence of Fano factors on firing rates. Error bars indicate SEM.

(C) Distribution of noise correlations.

(D) Dependence of noise correlations on geometric mean firing rates.

awake), we repeated the analysis on the anesthetized data using only the first 500 ms of the response (Figure 3F, dashed line), which reproduced the result obtained with the full response. Generally, the fraction of VE was substantially higher for cells with high firing rates (Figure 3F) and increased with the size of the window over which spikes were counted (Figure 3G). This effect was particularly strong under anesthesia, but much less so during wakefulness.

To gain insights into the structure of variability induced by the network state variable, we analyzed the key parameters of the model: weights and timescale. The weight of a cell tells us how the network state affects its firing rate. If all cells are comodulated in the same direction, we expect mostly positive weights and, thus, positive correlations between cells. If, on the other hand, some cells are enhanced (positive weights) while others are suppressed (negative weights), we expect mostly positive correlations within each group and negative correlations across groups. During wakefulness the weights were mostly distributed around zero (Figures 4A and 4C; 65% positive), while during anesthesia most weights were positive (Figures 4B–4D; 88% positive). Note, though, that there is an ambiguity in the GPFA model: one can always flip the sign of all weights without changing the model by simply flipping the sign of the latent variable (see Equation 1). By convention, we set the sign such that the majority of weights for each model are positive. We therefore expect a fraction greater than 50% to have positive sign, even in the absence of any effect (bootstrap 95% confidence intervals under the null hypothesis were as follows: awake 61.6%–62.9% positive weights and anesthetized 59.2%–60.4%). Thus, although it was significant ($p = 2 \times 10^{-9}$), only marginally more neurons than expected by chance had positive weights during wakefulness. Together with the finding above that the model explained very little variance, this indicates that there were no strong state fluctuations in our data during wakefulness. Under anesthesia, in contrast, the weights were mostly positive ($p < 10^{-15}$), indicating that the firing rates of most cells were comodulated by a common term, which presumably caused the elevated correlations observed above (Figures 2B and 2C) (we will quantify below what fraction of the correlations is accounted for by the network state variable).

The inferred timescale can help us to constrain our hypotheses on the origin of the observed correlations. If the common noise was due to shared sensory noise (Zohary et al., 1994; Shadlen and Newsome, 1998), then its time constant should be relatively small, corresponding roughly to the membrane time constants of the postsynaptic cells (10–50 ms) (Mason et al., 1991; Shadlen and Newsome, 1998). On the other hand, intrinsically generated up and down states, which have been observed with many non-opioid anesthetics, are much slower (<2 Hz) (Renart et al., 2010; Constantinople and Bruno, 2011; Haider et al., 2013). More consistent with the latter hypothesis, the timescale of the network state dynamics during anesthesia was relatively slow. The median width of the Gaussian temporal kernel was 207 ms (Figure 4F). In the frequency domain this corresponds to a low-pass cutoff frequency of 2.35 Hz (at −40 dB attenuation). This estimate of the timescale appears somewhat higher than that previously reported for anesthetized monkey V1 (Smith and Kohn, 2008). However, this difference is caused by what appears to be a bias in their method of estimating the timescale, rather than reflecting a discrepancy between the two data sets (performing the same analysis as they did showed that our data set is consistent with theirs; see Supplemental Information for an in-depth discussion of this issue). During wakefulness, in contrast, a large fraction of timescale values were around 800 ms (Figure 4E; median 688 ms), which is substantially longer than a single trial (500 ms). As the model does not take into account correlations of the network state across trials, this indicates that the network state was essentially constant within a trial. Thus, the strongest common modulations the model picked up during wakefulness were, in addition to being much weaker, substantially slower than the state fluctuations we observed under anesthesia.

We next turned to the pairwise correlation structure and asked to what extent it was explained by the network state fluctuations. The raw correlation structure under anesthesia resembled that in previous reports of anesthetized monkey V1 (Kohn and Smith, 2005; Smith and Kohn, 2008). Raw noise correlations were strongest for pairs with high firing rates (Figure 5A) (see also Smith and Sommer, 2013) and high signal correlations (Figure 5B). Moreover, they decreased significantly with the spatial separation between cells (Figure 5C). To determine to what degree the GPFA model accounted for this correlation structure, we computed the residual correlations after accounting for the network state. This can be thought of as computing correlations by not only conditioning on the stimulus but also on the network state (see Renart et al., 2010). We found that the network state explained most of

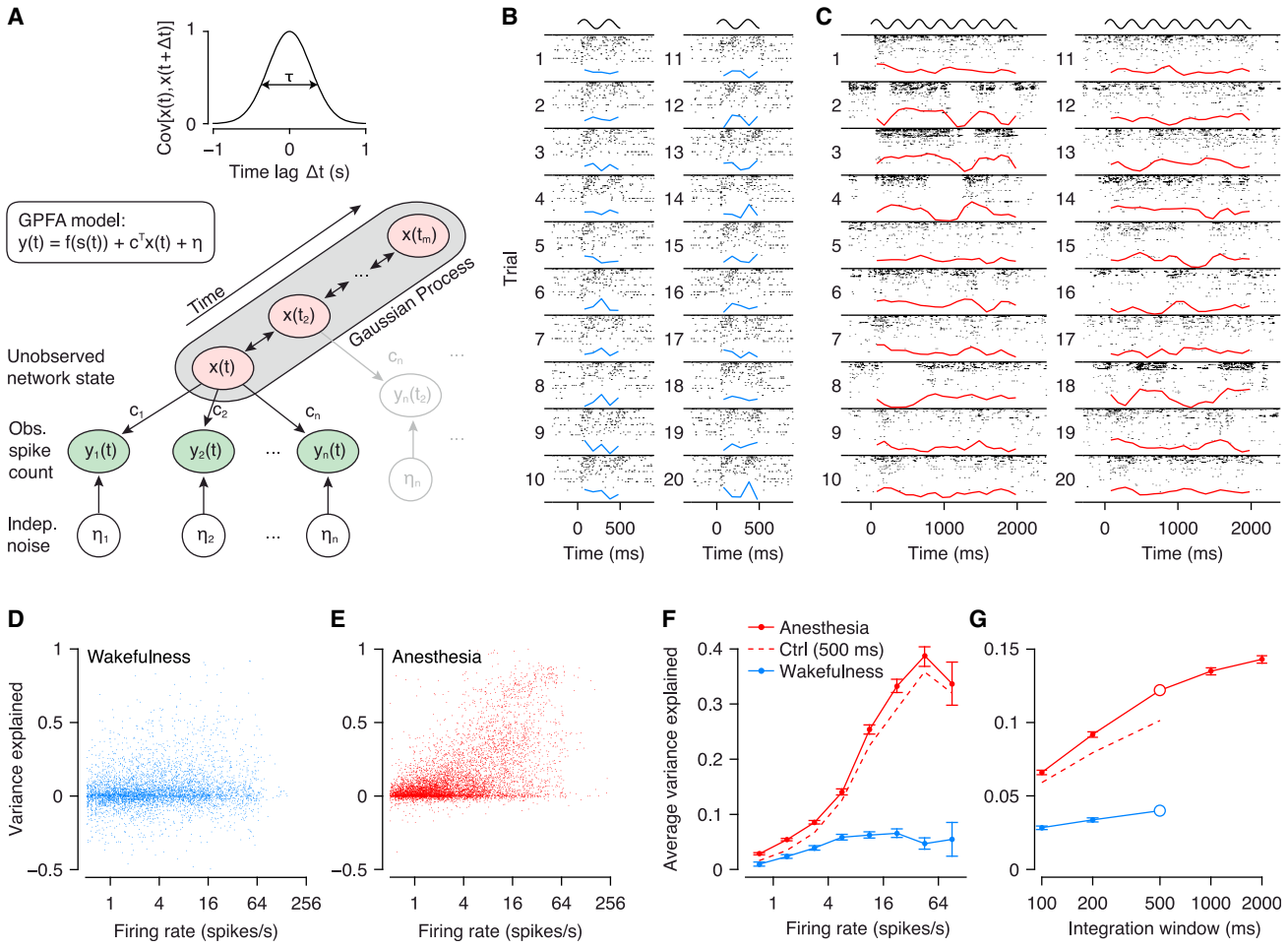

Figure 3. Gaussian Process Factor Analysis

(A) Schematic of the Gaussian Process Factor Analysis (GPFA) model. Spike count variability is generated by an unobserved (one-dimensional) network state (x) linearly driving neural activity (weights *c*) plus independent noise (η). The network state evolves smoothly in time, which is modeled by a Gaussian Process with temporal covariance shown at the top (correlation timescale τ is learned from the data).

(B) Population rasters for an example session recorded in an awake animal. Each numbered row shows the rasters of all recorded neurons during a single trial. All trials were under identical stimulus conditions (500 ms drifting grating, indicated by sine wave at the top). Blue line,estimate of the network state (x). The visible rate modulations are locked to the phase of the stimulus, but not to the estimated network state (which in this case had very little explanatory power).

(C) As in (B), but under anesthesia. The estimated network state captures the population rate dynamics very well (see, for example, trials 2–4) but is unrelated to the stimulus (stimulus duration: 2 s).

(D) Scatter plot of variance explained (VE) versus firing rate during wakefulness. Each dot is a single neuron under one stimulus condition. VE is computed in 500 ms windows.

(E) As in (D), but under anesthesia.

(F) Binned and averaged representation of (D) and (E). Error bars indicate SEM. Dashed lines indicate model fit on anesthetized data using only the first 500 ms of each trial for better comparison with awake data (error bars omitted for clarity; they were comparable to those for the solid red line).

(G) Average VE versus size of integration window. Open circles indicate 500 ms window, which was used for (D)–(F). Dashed line indicates control analysis as in (F).

the difference in the magnitude and structure of noise correlations between wakefulness and anesthesia. The residual correlation structure under anesthesia resembled the raw correlation structure during wakefulness remarkably well: except for pairs recorded on the same tetrode, the differences were within the margin of error (Figures 5A–5C). For pairs recorded on the same tetrode, the residual correlations under anesthesia were significantly higher than during wakefulness (Figure 5C; see Discussion). Accounting for network state did not alter the correlation structure during wakefulness. This finding was expected due to the low fraction of variance captured by the model during wakefulness (Figure 3F).

Model of State Fluctuations as Common Gain

The analysis of residual correlations showed that the correlation structure changed when accounting for network state: the firing rate dependence was nearly abolished (Figure 5A), and both the relation with signal correlations and with distance were

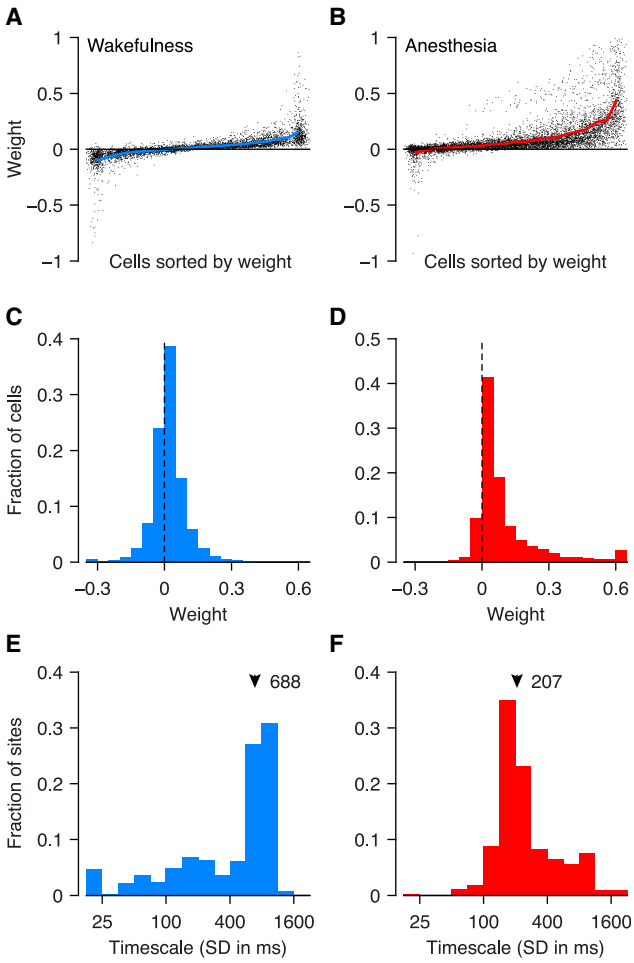

Figure 4. GPFA Model Parameters

(A–F) Distribution of weights (variable c, Equation 1) during wakefulness (A)–(C) and under anesthesia (B)–(D). Timescale of network state dynamics during wakefulness (E) and under anesthesia (F). The timescale is the SD (τ) of the Gaussian temporal correlation function of the latent variable (x) in the GPFA model.

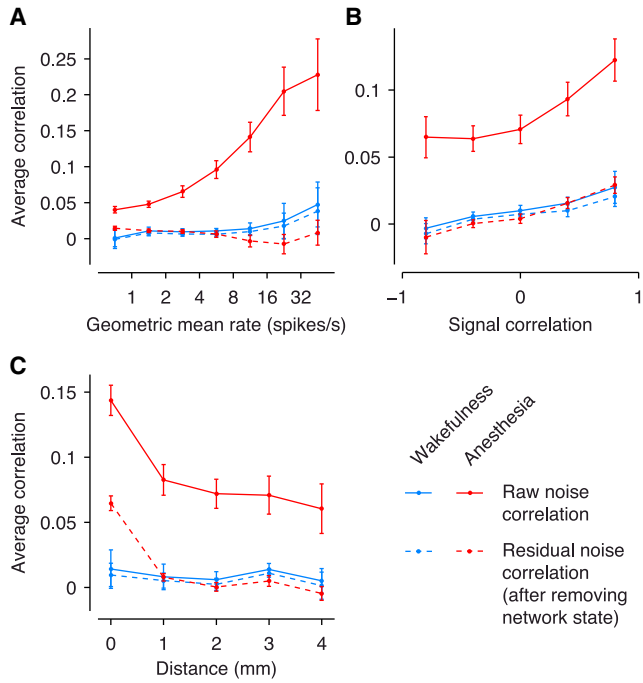

Figure 5. Accounting for Network State Reduces Noise Correlations under Anesthesia

(A–C) Raw (solid lines) and residual (after accounting for network state; dashed lines) noise correlations during wakefulness (blue) and under anesthesia (red). Dependence on firing rates (A), signal correlations (B), and distance between cells (C). Raw correlations in (A) are as in Figure 2D, except that here the model is fit for each condition separately. Error bars indicate SEM.

weakened substantially (Figures 5B and 5C). This may seem counterintuitive at first, since all neurons are modulated by the same common network state variable, and thus, one may expect a uniform effect on all neurons. However, since the network state can affect different neurons with different weights and those weights may depend on the stimulus, network state fluctuations can induce a nonuniform correlation structure. In our data, the weights were positively correlated with firing rates (data not shown), indicating that the network state acted as a common gain, modulating each neuron's firing rate multiplicatively.

To understand how such fluctuations in common gain would affect the correlation structure, we considered a simple network model: the firing rate of each neuron was determined by its tuning curve, which was multiplied by a common gain, and neurons spiked according to independent, inhomogeneous Poisson processes (Figure 6A; see Experimental Procedures for details). The gain term was fluctuating randomly with temporal correlations matching those in the data (~200 ms). This simple model was able to reproduce both the firing rate dependence of noise correlations in our data and their dependence on signal correlations quite naturally (Figures 6B and 6C). To capture the spatial dependence of correlations, we would have to include spatial structure (e.g., by replacing the global gain by one that can vary across space with a certain correlation structure). However, we do not pursue the question in more detail here, since the main point of the model is to illustrate that very simple mechanisms can cause remarkably nonuniform correlation structures. A similar model has been proposed recently by another group to model slow changes in excitability and their effect on response variability (Goris et al. 2013; see also Supplementary Material of Ecker et al., 2010).

Spontaneous Activity

We next asked whether the state fluctuations observed under anesthesia were also present during spontaneous activity in the absence of visual stimulation. To address this question, we analyzed the blank periods between subsequent stimulus presentations. The results essentially mirrored those obtained during visual stimulation (Figure 7). VE increased with both firing rates and the size of integration window (Figures 7A–7C). Weights were almost exclusively positive (96%, Figures 7D and 7E), and the timescale of the network state was comparable to that during visual stimulation (Figure 7F; median was 179 ms;

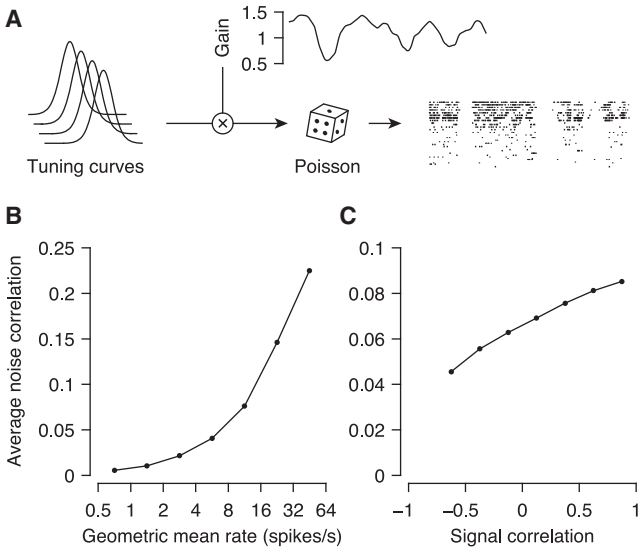

Figure 6. Model of State Fluctuations as Common Fluctuations in Excitability

(A–C) Illustration of the model. Cells have tuning curves with identical shapes and regularly spaced preferred orientations. Each cell's firing rate is given by the tuning curve multiplied by the common gain, which changes slowly as in our data. Spikes are generated by independent inhomogeneous Poisson processes with the given rates. The resulting noise correlations increase with firing rates (B) and signal correlations (C), as in the data.

cutoff frequency was 2.75 Hz). As for the evoked responses, residual correlations after accounting for network state were profoundly reduced (Figures 7H–7J).

Local Field Potential as a Predictor of Global Network State

We showed that under anesthesia most neurons are affected in a similar way by the network state, and this network state can change on a timescale of a few hundred milliseconds. If the effect is as global as it appears, we should find its signature in more global measures of neural activity, such as the local field potential (LFP). We thus asked whether the low-frequency range of the LFP correlated with the network state we inferred above. This was indeed the case for all three anesthetized, but for none of the awake, animals (Figures 8A and 8B). The magnitude of the correlation was strongest at zero time lag and had additional peaks/troughs of opposite sign at time lags of ±500 ms between LFP and inferred network state.

If the low-frequency range of the LFP is correlated with the network state, it should be possible to use it to predict the trial-to-trial variability observed under anesthesia. To verify this, we followed the approach taken by Kelly et al. (2010) and fitted a generalized linear model (GLM) with the low-pass-filtered LFP as input (see Experimental Procedures for details):

$$\mu(t) = \exp(a(t) + bu(t)). \quad (2)$$

Here $\mu(t)$ is the firing rate, $a(t)$ the stimulus response (PSTH), and $u(t)$ the LFP, all of which are functions of time. The linear weight b determines by how much a change in the LFP affects the firing rate of the neuron. During wakefulness the LFP weights were distributed mostly around zero (Figure 8C), whereas under anesthesia they were mostly negative (Figure 8D).

In summary, the network state we inferred above in an unsupervised way from spiking data alone (GPFA model) has its physiological counterpart in the low-frequency oscillations in the LFP. Both the low-frequency oscillations and the apparent network state fluctuations in the spiking activity of local populations are pronounced under anesthesia but relatively small, if not absent, during awake fixation.

Finally, our analysis so far has focused on comparing wakefulness and anesthesia using different cells recorded in different animals. However, anesthesia has multiple different stages, with light anesthesia being characterized by relatively desynchronized EEG activity, whereas deep anesthesia displays strong, coherent network oscillations. We therefore asked whether we could use the LFP to find evidence for slow changes in brain state (depth of anesthesia) within recording sessions. Indeed, in many sessions we observed slow changes in LFP power in a low-frequency range and sometimes in the gamma range (Figures 9A and 9B). To quantify these changes, we computed an LFP power ratio in windows of approximately 90 s (power at 0.5–2 Hz divided by that in the gamma band, 30–70 Hz) (Goard and Dan, 2009), which we used as a proxy for depth of anesthesia. This power ratio displayed changes on timescales of a few minutes up to half an hour and longer (Figures 9C and 9D, black lines). Remarkably, the time-resolved LFP power ratio was tracked very closely by the total correlation in the network as measured by the variance of the network state variable inferred by the GPFA model (Figures 9C and 9D, red lines). Across all sessions, the LFP power ratio and the overall level of correlations were significantly correlated (Figure 9E; Spearman's $\rho = 0.42$, $p < 10^{-15}$). This correlation was positive and significant in 19/27 individual sessions ($p < 0.05$, uncorrected). Thus, the degree of network-wide correlations varied within a recording session in the same cells over the course of several minutes and correlated well with more traditional, LFP- or EEG-based measures of brain state or depth of anesthesia.

DISCUSSION

State Fluctuations under Opioids

We demonstrated a striking feature of cortical activity under opioid anesthesia that had previously not been appreciated: neurons undergo spontaneous coordinated transitions between states of almost complete silence, highly elevated levels of activity, and intermediate levels of activity. These state transitions resemble up and down states, which have been described previously for other, nonopioid anesthetics (Steriade et al., 1993; Renart et al., 2010; Constantinople and Bruno, 2011), and they occur on a timescale of several hundred milliseconds. In addition, the strength of these state fluctuations can change slowly over several minutes, which may reflect slow changes in the depth of anesthesia.

Although the effect of opioid anesthetics may be less dramatic than that of nonopioids such as urethane, isoflurane, or ketamine (Constantinople and Bruno, 2011; Movshon et al., 2003; Kohn et al., 2009; Smith and Sommer, 2013), it should be emphasized

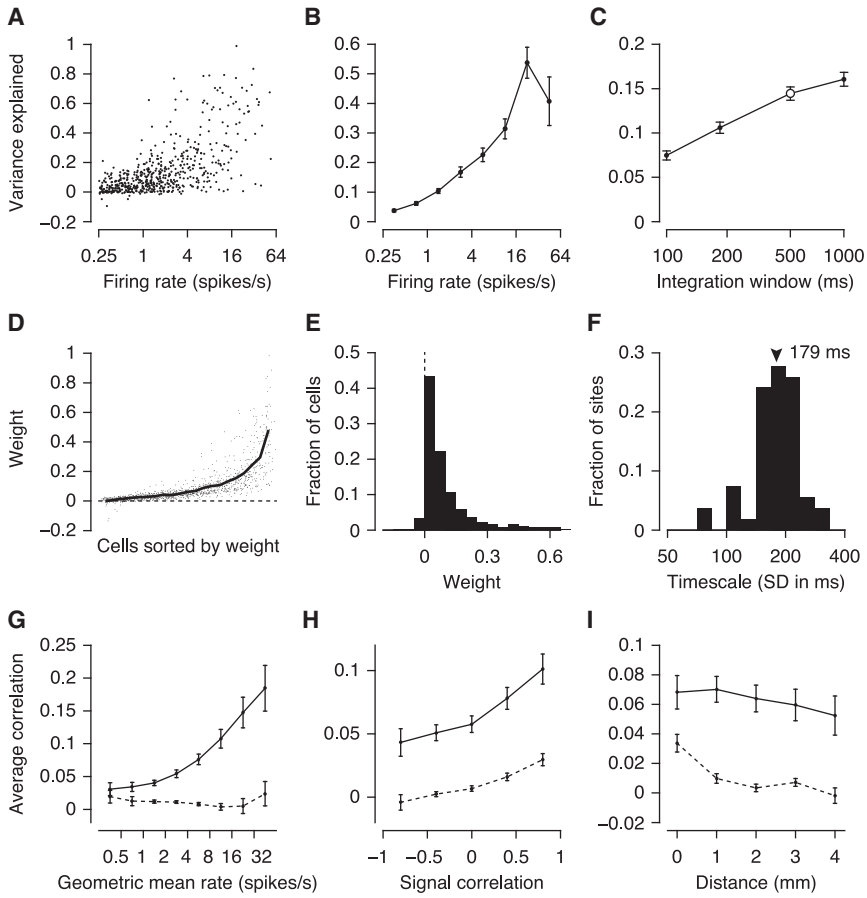

Figure 7. GPFA Model during Spontaneous Activity under Anesthesia

(A and B) VE versus firing rates (as in Figures 3D–3F).

(C) VE versus integration time (as in Figure 3G).

(D and E) Distribution of weights (as in Figures 4B–4D).

(F) Distribution of timescales (as in Figure 4G).

(G–I) Residual correlations versus firing rate, signal correlation, and distance, respectively (as in Figures 5A–5C).

that they still have a substantial effect on neural responses, explaining on average more than one third of the variance of cells firing at rates of more than 10 spikes/s (Figure 3). Since the effect is largely common to all cells within a few millimeters of cortex, it becomes particularly evident when considering populations of simultaneously recorded neurons and substantially biases the structure of noise correlations compared with awake recordings.

We are aware of two reports that directly addressed the effect of opioids and found no differences to the awake state (Loughnan et al., 1987; Constantinople and Bruno, 2011). Although they may superficially appear at odds with our results, this is not the case. One study measured the average sensory-evoked EEG response in humans (Loughnan et al., 1987) and found no difference between anesthetized and awake subjects. While this finding is consistent with our results that sensory responses were intact, it does not rule out spontaneous state transitions, as those would have been averaged out. The other study measured membrane potential fluctuations in single neurons (Constantinople and Bruno, 2011). It is possible that opioids act more subtly than other anesthetics, not inducing the bimodal distribution of membrane potentials that typically characterizes up and down states (Petersen et al., 2003; Constantinople and Bruno, 2011), but nevertheless leading to global fluctuations in spiking output that are strong enough to be picked up when recording populations of neurons simultaneously. Another important point to be noted is that the two studies cited above were conducted under much lighter anesthesia. The fentanyl doses used (3 μg/kg bolus and 10 μg/kg/hr, respectively) were substantially lower than the minimum equivalent sufentanil dose used in acute primate experiments (our study, Smith and Kohn, 2008, and Kelly et al., 2010: 4–15 μg/kg/hr sufentanil, equivalent to 40–150 μg/kg/hr fentanyl). Thus, the differences in depth of anesthesia, different measures of neural activity, or differences between species could account for the differences between these studies and ours.

State Fluctuations during Wakefulness

State transitions similar to those we observed under anesthesia have been observed in rodents also during wakefulness. Poulet and Petersen (2008) found that periods of inactivity (termed quiet wakefulness) resembled the anesthetized state. Both the intracellular membrane potentials and the LFP displayed increased power in the low frequencies, similar to our and other labs' findings under anesthesia, and spikes were tightly locked to those oscillations. During periods of active whisking, in contrast, somatosensory cortex was in a desynchronized state that resembled our awake results. In addition, Niell and Stryker (2010) showed that the firing rates of neurons in primary visual cortex of mice depend strongly on whether the mouse is still or running on a treadmill. Although they did not explicitly test whether response variability or properties of the LFP were different between the two states, their findings support the idea that the cortex can switch between different states of activity during wakefulness.

While slow changes in excitability of single neurons and populations have been reported (Bair et al., 2001; Goris et al., 2013), state fluctuations occurring at the timescale of a few hundred milliseconds have to our knowledge not been observed in the visual system of awake, behaving primates. One could speculate that this is due to a species difference between rodents and primates. However, it seems more likely that we did not observe such quiet states during our awake experiments because the monkeys had to actively initiate a trial by moving their eyes to the fixation spot and maintain fixation throughout the trial, actively suppressing their natural reflex to move the eyes several

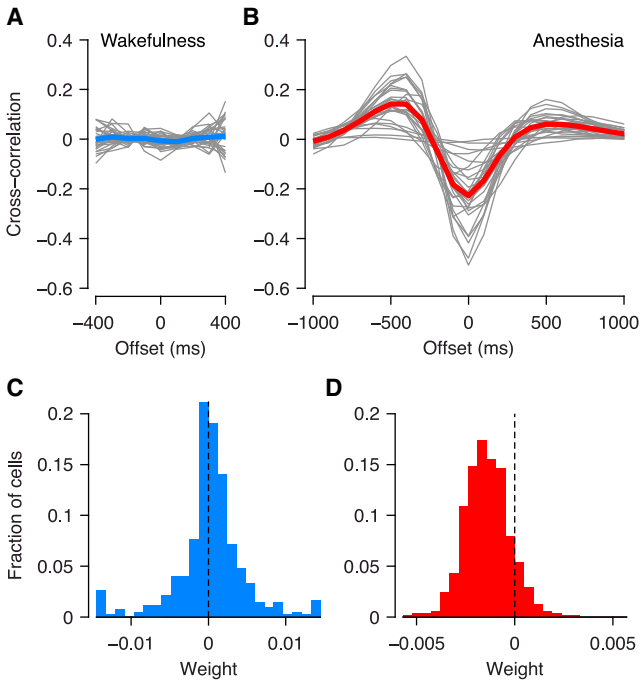

Figure 8. Local Field Potential Is Correlated with Inferred Network State and Predicts Trial-to-Trial Variability under Anesthesia but Not during Wakefulness

(A) Cross-correlation between low-frequency LFP (0.5–5 Hz) and network state inferred by GPFA model during wakefulness. Gray lines indicate individual sessions; blue line indicates average across all sessions.

(B) As in (A), but under anesthesia.

(C) Distribution of LFP weights in Generalized Linear Model taking stimulus and LFP into account; during wakefulness.

(D) As in (C), but under anesthesia.

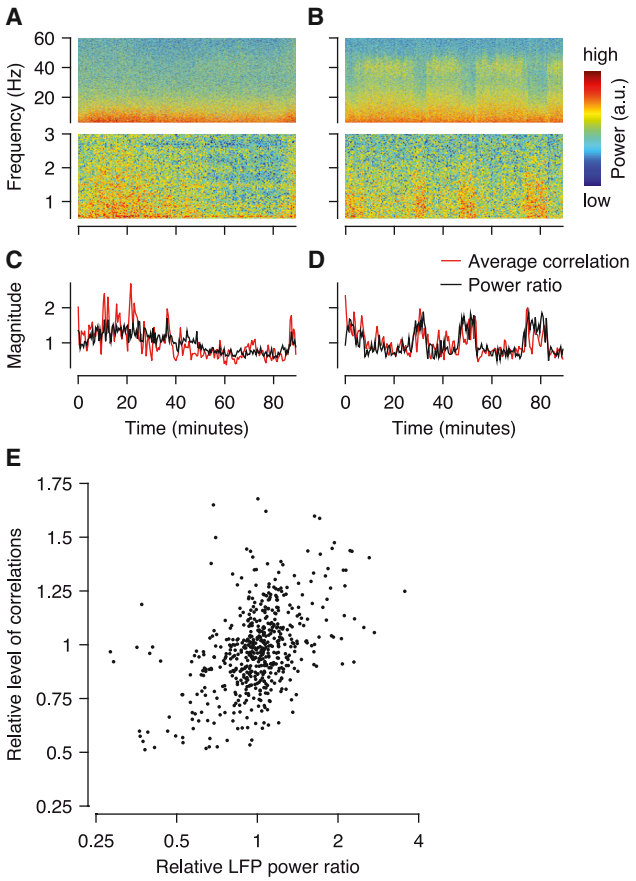

Figure 9. LFP Power Ratio Correlates with Overall Level of Noise Correlations

(A and B) Spectrogram of LFP over the course of two example recordings (~90 min).

(C and D) LFP power ratio (black line, power in 0.5–2 Hz band divided by that in the gamma band, 30–70 Hz) and average level of correlations (red line, variance of the network state inferred by GPFA) for the same sessions. Both quantities are normalized by the session average.

(E) Population analysis. LFP power ratio versus overall correlation (variance of network state inferred by GPFA) in 20 separate blocks per recording (27 recordings in total; i.e., n = 540). Both quantities normalized by the session average for each session. One outlier cropped for clarity.

times per second. This required oculomotor action before and during the stimulus could trigger an active state similar to whisking or running in rats and mice.

This action to initiate a trial may be an important difference between experiments in the visual system of awake monkeys and rodents. Unlike with monkeys, in most studies of the rodent visual system the animals do not have to actively initiate a trial, but stimuli are presented periodically. To obtain a similar level of control over the brain state, one would have to either infer it post hoc from recordings of locomotion, eye, or whisker movements or—as we did in this study—directly from neuronal population activity. Since this is not usually done (but see Poulet and Petersen, 2008; Niell and Stryker, 2010), many data sets collected in awake rodent visual cortex are likely to contain a mixture of brain states. We, therefore, do not expect large differences between wakefulness and anesthesia in such cases, a hypothesis corroborated by a recent study of noise correlations in mouse V1 (Denman and Contreras, 2013).

Role of Firing Rates

Could the difference between our awake and anesthetized data be attributed to factors other than anesthesia? It has been suggested that the low correlations we measured in awake monkeys were a result of unusually low firing rates (Cohen and Kohn, 2011). However, this is not a viable explanation since firing rates were similar in our awake and anesthetized recordings, and they were comparable to (in fact, slightly higher than) those reported by other labs using similar stimuli in the same cortical area as in our present study (Smith and Kohn, 2008: 3.4 spikes/s; this study, awake: 5.4 spikes/s and anesthetized: 5.0 spikes/s). In addition, the difference between awake and anesthetized correlations was evident at the full range of firing rates (Figure 2), and the firing-rate dependence of correlations in our anesthetized data set resembled that reported by other labs in anesthetized monkey V1 (Smith and Kohn, 2008; Smith and Sommer, 2013). In summary, while firing rates certainly contribute to differences between studies to some extent, they cannot account for the difference between wakefulness and anesthesia.

Role of Cortical Layers

Recent studies suggest that noise correlations are low in the granular layers of V1, raising the possibility that our awake recordings were mostly restricted to those layers (Hansen et al., 2012; Smith et al., 2013). If this was the case, the effects we describe in this study could be caused by laminar differences, rather than reflecting a difference between wakefulness and anesthesia. Based on our data, we cannot rule out this possibility entirely, but a number of observations argue against it. Although in our anesthetized experiments we recorded throughout all layers and tried to adjust all tetrodes to a similar depth for each recording, we were unable to identify the region of low correlations. This is most likely owed to the limitations of our experimental approach. Tetrodes have a blunt tip, presumably causing more tissue displacement than single electrodes with small, beveled tips, making the point of entry into the brain a poor reference to estimate laminar location. In addition, we did not reach white matter with all tetrodes before the end of the experiment, precluding the use of white matter as a reference. Furthermore, tetrodes have much lower impedances than single electrodes. Therefore they probably sample cells from a larger volume. We thus expect considerable variability in both the laminar location of the tetrodes and our estimates thereof. Since the region of low correlations reported previously (Hansen et al., 2012; Smith et al., 2013) is a narrow strip of 200–300 μm, it may not be surprising that we were unable to identify it. However, for the same reasons it seems implausible that laminar variation should explain the low correlations we observed during wakefulness. For this to be the case, most of our tetrodes should have been located in exactly this narrow region. Yet, unlike in our anesthetized experiments, we neither adjusted the tetrodes together nor did we target any specific layer, but instead we adjusted each tetrode to a position where it isolated cells. In addition, between awake recording sessions we sometimes adjusted the tetrodes, in total by up to 600 μm (median was ~300 μm) between the first and the last experiment. As a result, we should either have been able to localize the region of low correlations during anesthesia or we likely recorded from outside it as well during wakefulness, suggesting that the effect we describe is not simply explained by laminar differences.

Relation to Other Studies of Noise Correlations in the Primate Visual System

By modeling the state fluctuations under anesthesia with a latent variable model (GPFA), we recovered the residual correlation structure, which was remarkably similar to that observed in the awake monkey. This finding reconciles the results of previous studies conducted in V1 under anesthesia with our awake, fixating data (Ecker et al., 2010). The raw correlation structure we observed under anesthesia is entirely consistent with previous reports using the same preparation (Kohn and Smith, 2005; Smith and Kohn, 2008). The higher average level of correlations during anesthesia (Reich et al., 2001; Kohn and Smith, 2005; Smith and Kohn, 2008) is accounted for by the one-dimensional network state variable. The LFP can be used to predict some of these state fluctuations under anesthesia, which has been reported previously (Kelly et al., 2010). Interestingly, recent work suggests that much slower changes in excitability (on the order of minutes)—which we explicitly excluded from our analysis—are also stronger under anesthesia than during wakefulness (Goris et al., 2013). Finally, another study characterizing higher-order correlations in anesthetized monkey V1 (Ohiorhenuan et al., 2010) reports an excess probability of silence in triplets of neurons, suggesting that the periods of almost complete silence we observe are also present in other anesthetized preparations.

Some discrepancies remain between the papers discussed above (Kohn and Smith, 2005; Smith and Kohn, 2008; Reich et al., 2001; Ohiorhenuan et al., 2010; Ecker et al., 2010) and some other studies. For instance, some authors report substantially higher noise correlations in awake monkey V1 (0.2–0.4) (Gutnisky and Dragoi, 2008; Hansen et al., 2012; Herrero et al., 2013) than we did (Ecker et al., 2010). Note that in addition to substantially higher average firing rates, these studies typically also observed relatively high Fano factors ($F > 2$; Gutnisky and Dragoi, 2008; Herrero et al., 2013; our awake data: average $F = 1.1$, Figure 2A), indicating that either different cell populations were sampled or additional confounding factors were present that were not accounted for (e.g., as argued in Ecker et al., 2010; Bair et al., 2001). For instance, accounting for eye movements reduced the correlations by almost 50% in Hansen et al. (2012) (their Figure S3).

Correlations between Nearby Neurons

Similar to other authors (e.g., Smith and Kohn, 2008; Cohen and Maunsell, 2009), we focused mainly on pairs recorded by different electrodes. For such pairs, accounting for the network state under anesthesia reduced the noise correlations consistently below 0.01, similar to the level observed during wakefulness. However, a notable observation we made was that residual correlations between pairs recorded by the same tetrode were still higher under anesthesia than during wakefulness (Figure 5C). This could reflect an additional, more local contribution of anesthesia that was not captured by the single latent variable in our model. Alternatively, there may be some degree of heterogeneity in the local connectivity, which gives rise to different levels of correlation depending on where one records from (e.g., close to pinwheels versus linear zones or differences between layers). Indeed, when we reanalyzed the awake data, focusing on pairs recorded by the same tetrode, we observed some differences between the two monkeys. In one monkey, signal correlations for pairs recorded on the same tetrode were close to zero (average 0.025) and so were the noise correlations (average 0.006), while in the other monkey signal correlations were positive (0.24) and noise correlations were somewhat higher as well (0.045). The latter is more consistent with the anesthetized results (average signal correlations: 0.17; average residual noise correlations: 0.065). It is possible that we sampled cells in a more unbiased fashion in our anesthetized experiments, in which we recorded from more monkeys and more individual tetrodes than in our awake data set. To reach a definite conclusion regarding the structure and level of correlations for neurons separated by less than 200 μm and to resolve the potential contribution of cortical layers, more extensive future experiments with high-density laminar probes (Blanche et al., 2005) are needed.

CONCLUSIONS AND FUTURE DIRECTIONS

Most of what we know today about the early visual system we learned through studies in anesthetized animals (e.g., Hubel and Wiesel, 1968; Zeki, 1974; De Valois et al., 1982a, 1982b; Movshon et al., 1985; Carandini et al., 1997). The acute anesthetized preparation is undoubtedly an extremely valuable tool that offers many advantages for studying the early visual system (no training of animals, no issues due to eye movements/microsaccades, longer experiments with more trials, etc.). For instance, receptive fields or tuning curves can be measured under anesthesia just as well as in the awake animal.

More recently, however, many groups have started to characterize the joint activity patterns of pairs and groups of neurons (Zohary et al., 1994; Gawne and Richmond, 1993; Gawne et al., 1996; Bair et al., 2001; Reich et al., 2001; Kohn and Smith, 2005; Smith and Kohn, 2008; Gutnisky and Dragoi, 2008; Ecker et al., 2010; Berens et al., 2012), and both the origin and the implications of neuronal correlations have been of great interest (Zohary et al., 1994; Shadlen and Newsome, 1998; Abbott and Dayan, 1999; Sompolinsky et al., 2001; Averbeck et al., 2006; Cohen and Newsome, 2008; Josić et al., 2009; Nienborg and Cumming, 2009; Ecker et al., 2011). For these studies it is important to distinguish between different sources of correlation: if the network transitions from one state to another, such widely distributed dynamics can quickly become the dominant source of (co)variance. However, if such state transitions do not occur in alert animals paying attention to or interacting with their environment, the functional relevance of these correlations may be very different from those originating from shared input in the feed-forward signal chain of upstream neurons. Thus, one should be aware of possible state fluctuations and, if necessary, take them into account. While some authors have done so by considering only data during those periods where the brain was in a certain state (e.g., Renart et al., 2010) or incorporating global signals such as the LFP directly into the response model (Kelly et al., 2010), our study showed that in some situations the network state may also be inferred directly from population data using a latent variable model (Figures 3–5).

Latent variable models like the one we used in this study (GPFA, Yu et al., 2009; see also Macke et al., 2011; Buesing et al., 2012) are powerful tools for future studies of neuronal population activity. In light of current and future technological developments, the number of neurons that can be monitored simultaneously will increase substantially. The amount of time that can be used to collect data, however, is and remains limited by experimental and ethical constraints. Thus, an accurate characterization of the joint population response will be feasible only if much of the variability is restricted to a relatively low-dimensional subspace. Fortunately, this is very likely to be the case if our original hypothesis is correct and most of the correlations observed in awake animals are driven by unobserved internal signals rather than by shared sensory noise (Ecker et al., 2010). In this case, latent variable models will not only afford a parsimonious statistical description of neuronal population data, but they may also provide us with a method to read out internal signals, such as the focus of attention (Cohen and Maunsell, 2010), task strategies, or many more, in real time on a trial-by-trial basis.

EXPERIMENTAL PROCEDURES

Electrophysiology in Awake Monkeys

We recorded from two adult, male rhesus monkeys (*macaca mulatta*) using chronically implanted tetrode arrays. The awake data set used in this study is a subset of a data set analyzed previously (Ecker et al., 2010; Berens et al., 2012) (see below for inclusion criteria). Surgical methods and recording protocol for our awake experiments have been described previously (Tolias et al., 2007; Ecker et al., 2010).

Electrophysiology in Anesthetized Monkeys

In acute experiments lasting 4–5 days, we recorded from three adult, male rhesus monkeys (*macaca mulatta*) using the same 24-tetrode arrays as in the awake recordings. Surgical details are described in the Supplemental Experimental Procedures. Prior to each set of recordings, all tetrodes were adjusted to a new target depth approximately 200 μm deeper than the previous one. The exact amount of adjustment varied by tetrode, leaving tetrodes (if possible) at a position where cells could be isolated. Throughout the experiments anesthesia was maintained by intravenous infusion of sufentanil (4–15 μg/kg/hr; protocol similar to Kohn and Smith, 2005; Smith and Kohn, 2008). Animals were paralyzed using vecuronium bromide by intravenous infusion (100 μg/kg/hr). The pupils were dilated by topical application of cyclopentolate. Refraction was provided by contact lenses. Stimuli were presented monocularly; the other eye was closed and covered. The open eye was kept irrigated using saline. Vital signs (ECG, heart rate, respiratory rate and volume, blood pressure, temperature, CO_2, O_2, and SpO_2) were monitored continuously. All experimental procedures complied with guidelines approved by the Baylor College of Medicine Institutional Animal Care and Use Committee (IACUC).

Visual Stimuli/Behavioral Paradigm

Visual stimuli were drifting gratings (16 different directions of motion) under a circular aperture presented at full contrast on gray background using the Psychophysics toolbox for Matlab (Brainard, 1997). In a subset of awake experiments, stimuli were static gratings (eight orientations), partly at lower contrasts (see Ecker et al., 2010 for details). Because of space constraints in the anesthetized setup, we used an LCD monitor running at a refresh rate of 60 Hz and positioned at a distance of 55 cm to the eye during our anesthetized experiments. The stimuli for awake monkeys were presented on CRT monitors running at 100 Hz and positioned at a distance of 100 cm. To address concerns previously raised about low firing rates in our data (Cohen and Kohn, 2011), we reduced the size of the stimuli during the anesthetized experiments to 2°–3° in diameter, compared with 4° in awake experiments. We ensured that the gratings covered the receptive fields of all neurons by mapping multiunit receptive fields of most tetrodes manually before each recording session. Temporal frequency was 3.4 cycles/sec for all sessions. Spatial frequency varied between 3–6 cycles/deg, roughly matching the preferences of the recorded cells due to some variability in eccentricity of recording locations (estimated between 1°–4° from the fovea). Stimulus conditions were randomized in blocks of 16 trials to ensure a balanced number of repetitions.

In awake experiments, trials were initiated by a sound and the appearance of a fixation target (~0.15°). After the monkey fixated for 300 ms, the stimulus was shown for 500 ms, and the monkey had to fixate for another 300 ms. Monkeys were required to fixate within a radius of 0.5°–1°, but typically fixated much more accurately, as revealed by offline analysis. Monkeys were rewarded by a drop of juice upon completion of a successful trial.

In anesthetized experiments, stimuli were shown for 2 s, separated by blank periods with a gray screen lasting approximately 1.1–1.6 s (randomly drawn from a uniform distribution).

Spike Detection and Sorting

Our data processing methods are based on previously published work (Tolias et al., 2007) but have been revised since the original report. A detailed description can be found in the Supplemental Experimental Procedures. Briefly, spikes were detected offline when the signal on any of the four channels crossed a threshold of five times the SD of the noise. After spike alignment, we extracted the first three principal components on each channel, resulting in a 12-dimensional feature vector used for spike sorting. To deal with

waveform drift, we fit a mixture model that uses Kalman filters to track changing cluster means over time (Calabrese and Paninski, 2011). Single unit isolation was assessed quantitatively using the mixture model. Since the focus of this paper is on global fluctuations that are distributed among many tetrodes, spike-sorting errors are unlikely to play an important role; they would affect primarily pairs recorded by the same tetrode (Ecker et al., 2010). Therefore, we included all units flagged as single units in the analysis to increase statistical power. The sum of the false positive rate and the false negative rate was less than 10% for 62% of the single units in our data set and less than 20% for 83% of the single units (awake: 63% and 82%; anesthetized: 61% and 83%).

Data Set and Inclusion Criteria

We recorded from two awake and three anesthetized monkeys, a total of 46 and 30 recording sessions, respectively. We included recording sessions where gratings were shown for at least 500 ms per trial, at least 20 trials per condition, and at least 10 single units with stable firing rates were recorded. Firing rate stability was assessed by computing the long-term component of the trial autocorrelogram (Bair et al., 2001), which we estimated by taking a weighted average (Gaussian window with SD of eight trials) around zero, excluding the bin at zero lag (which is one by definition). Units were considered stable if the long-term component of the trial-autocorrelation was less than 0.1. These criteria resulted in 31 awake and 27 anesthetized recording sessions with 487 and 636 single units, respectively. The stability criterion was important since the anesthetized experiments were performed acutely and tetrodes were adjusted every 8–10 hours. Due to this criterion we excluded 73 of 560 cells (13%) from our awake dataset and 293 of 929 cells (32%) from our anesthetized dataset. An obvious consequence of this procedure is that drifts in firing rates over slow timescales (Goris et al., 2013), possibly due to physiological reasons, would not be recovered by our analysis even if they are common to multiple cells (see Supplemental Experimental Procedures for a discussion).

Data Analysis/Availability of Code and Data

Data analysis was done in Matlab using a data analysis framework with MySQL database backend (DataJoint: https://github.com/datajoint; D. Yatsenko, Tolias Lab, Baylor College of Medicine). The complete data set, and code used for data processing, data analysis, and creating the figures in this article are available at http://toliaslab.org/publications/ecker-et-al-2014.

Orientation Tuning

We assessed the significance of orientation tuning by a permutation test. We first extracted the magnitude of the second Fourier component (i.e., orientation) by projecting the vector of average responses for each orientation onto a complex exponential with two cycles:

$$q = \sum_{k=1}^{16} \langle r \rangle_k \exp\left(\frac{\pi i k}{4}\right), \tag{3}$$

where $\langle r \rangle_k$ is the average response to the k^{th} direction of motion. We compared $|q|$ to its null distribution, which we obtained by shuffling the trial labels. We ran 1,000 iterations of the shuffling procedure and used the fraction of runs with $|q|$ greater than that observed in the real data as the p value.

Fano Factors/Noise Correlation Analysis

Fano factors and noise correlations were computed on the first 500 ms of the response for both awake and anesthetized experiments. Fano factors were computed as the variance of the spike count divided by its mean. Noise correlations were computed as the Pearson correlation coefficient of two neurons' responses to identical repetitions of the same stimulus condition, averaged (for each pair) over all stimulus conditions with nonzero firing rates in both neurons.

GPFA

A detailed description of the GPFA model and the derivation of the Expectation Maximization (EM) algorithm to fit it can be found in Yu et al. (2009). Here we describe only the key points.

The GPFA model is described in the main text (Equation 1; Figure 3). We extracted spike counts in each trial during the stimulus period in T nonoverlapping bins of 100 ms starting 30 ms after stimulus onset (awake: $T = 5$, anesthetized: $T = 20$). We square-root-transformed spike counts to stabilize the variances (Yu et al., 2009). Before fitting the model, we subtracted the average across trials for each stimulus condition and time bin. This procedure removes systematic contributions by the stimulus, and thus, the model explains only the trial-to-trial variability. Note that in this case both the network state x and the observed (transformed) spike counts $\boldsymbol{y}$ have zero mean (over trials) in each bin. The noise covariance under this model is given by

$$\mathrm{Cov}[\boldsymbol{y}] = \boldsymbol{c}\boldsymbol{c}' + R, \tag{4}$$

where the prime ($'$) denotes the transpose, $\boldsymbol{y}$ are the square-root-transformed and mean-subtracted spike counts, $\boldsymbol{c}$ is a vector of linear weights mapping network state to firing rate, and R is a diagonal matrix of residual (independent) variances. We fitted the model for each stimulus condition independently to allow the weights to depend on the stimulus (this was indeed the case; weights increased with firing rates, which was reflected in both the increase of correlations and VE with firing rates, Figures 2 and 3). Units were included in the model in all stimulus conditions where they fired at least 0.5 spikes/s during the stimulus period.

The network state x was assumed to evolve smoothly in time. This was achieved by modeling its temporal correlations by a Gaussian kernel

$$K_{ij} \equiv \mathrm{Cov}[x(t_i), x(t_j)] = \exp\left(-\frac{(t_i - t_j)^2}{2\tau^2}\right). \tag{5}$$

To keep the algorithm computationally tractable, we set temporal correlations in network state extending across trials to zero.

To evaluate the fraction of variance explained (VE) (Figure 3) and the residual correlations (Figure 5), we used an independent test set that had not been used for fitting the model. Training and test set consisted of the first and second half of the data (and vice versa; i.e., 2-fold cross-validation). We fit the model on spike counts in 100 ms windows, but residual correlations and VE can also be evaluated for larger counting windows by summing up variances and (temporal) covariances over several time bins. VE (Figure 3) and residual noise correlations (Figure 5) were calculated for 500 ms windows, since this was the maximum available in the awake data set. For details on how to compute VE and residual correlations, see Supplemental Experimental Procedures.

Model of Common Gain Modulation

The model population (Figure 6) consisted of 64 neurons with uniformly spaced preferred orientations and von Mises tuning curves given by

$$f_k(\theta) = \exp(\kappa \cos(2(\theta - \varphi_k)) + \alpha), \tag{6}$$

where φ_k is the preferred orientation, $\kappa = 2$, and $\alpha = 1.8$, resulting in a bandwidth of ~25° (half-width at half-maximum) and a peak firing rate of 45 spikes/s. The firing rate of each neuron was determined by the product of its tuning curve and the value of the common gain

$$\mu_k(t) = g(t) \cdot f_k(\theta). \tag{7}$$

The gain had $\mathrm{E}[g] = 1$ and its temporal autocorrelation was a Gaussian kernel

$$K_{jk} \equiv \mathrm{Cov}[g(t_j), g(t_k)] = \sigma^2 \exp\left(-\frac{(t_j - t_k)^2}{2\tau^2}\right), \tag{8}$$

with $\sigma = 0.15$ and $\tau = 200$ ms. We sampled independent Poisson spike counts from the given rates $\mu(t)$. As for the data, we used bins of 100 ms and computed correlations in bins of 500 ms.

Analysis of Spontaneous Activity under Anesthesia

For the analysis of spontaneous activity (Figure 7), we used the blank periods between two subsequent stimuli. We analyzed segments of 1 s duration starting 200 ms after the end of the stimulus (to avoid contamination by off responses to the stimulus). Approximately 75% of the blank periods were long enough to be included given these criteria, resulting in an average of 1,188 "trials" (min: 1,148; max: 1,225).

GLM Accounting for Network State

Following Kelly et al. (2010), we fitted a GLM with the low-pass-filtered LFP as input (Figure 8). The model is defined in Equation 2 in the main text. As for the GPFA model above, we used spike counts in 100 ms bins and fitted the model independently for each stimulus condition. The contribution of the stimulus was captured by the parameter $a(t)$, which represents the PSTH. The LFP predictor $u(t)$ was the bandpass-filtered (0.5–5 Hz) LFP. We averaged the LFP over all tetrodes that recorded at least one single unit in this session and subtracted the average stimulus-evoked response. The latter ensured that LFP weights captured only fluctuations around the average response to the stimulus. For analysis of the weights (Figures 8C and 8D), we averaged the weights of each neuron across all conditions in which it was included (firing rate >0.5 spikes/s). The cross-correlation between LFP and network state estimated by GPFA (Figures 8A and 8B) was computed by first subtracting the average of each measure within each trial (i.e., it is the correlation of the fluctuations within trials rather than across trials).

Analysis of Depth of Anesthesia

To assess slow changes in brain state, we performed spectral analysis on the LFP (Figure 9). We averaged the LFP across all tetrodes that recorded at least one single unit in this session and computed the spectrogram using 200 overlapping windows (16 trials or ~1 min per window, with 50% overlap). The spectrogram was computed on the continuous LFP trace including both evoked and spontaneous activity; no average stimulus response was subtracted. Following Goard and Dan (2009), we computed a power ratio to assess brain state. The power ratio was defined as the power in the low-frequency band (0.5–2 Hz) divided by that in the gamma band (30–70 Hz). To quantify the overall correlation in the network, we computed the variance of the network state variable inferred by the GPFA model in the same windows as we used for the spectral analysis above. For the population analysis (Figure 9E), we used 20 nonoverlapping windows to quantify both the power ratio and the overall correlation. This smaller number was chosen as a trade-off between temporal resolution and reducing noise by including more data.

SUPPLEMENTAL INFORMATION

Supplemental Information includes three figures and Supplemental Experimental Procedures and can be found with this article online at http://dx.doi.org/10.1016/j.neuron.2014.02.006.

ACKNOWLEDGMENTS

We thank Dennis Murray, Tori J. Shinn, Allison N. Laudano, Amy M. Morgan, Jessica L. Rudy, and Wangchen Wang for technical assistance and help with data collection; Byron Yu and John P. Cunningham for sharing their GPFA code; Sven Simon and Rahul G. Baijal for discussion and consultation with anesthesia; Dimitri Yatsenko for discussion and the development of DataJoint; and Ralf M. Haefner for comments on the manuscript.

This work was supported by grants NEI R01-EY018847, NEI P30-EY002520-33, and the NIH-Pioneer award DP1-OD008301 to A.S.T.; the McKnight Scholar Award to A.S.T; the Bernstein Center for Computational Neuroscience (FKZ 01GQ1002); the German Excellency Initiative through the Centre for Integrative Neuroscience Tübingen (EXC307); an HHMI Early Career Award to S.S.; and NEI R01-EY019272 to S.S.

Accepted: January 28, 2014
Published: April 2, 2014

REFERENCES

Abbott, L.F., and Dayan, P. (1999). The effect of correlated variability on the accuracy of a population code. Neural Comput. *11*, 91–101.

Angel, A. (1993). Central neuronal pathways and the process of anaesthesia. Br. J. Anaesth. *71*, 148–163.

Averbeck, B.B., Latham, P.E., and Pouget, A. (2006). Neural correlations, population coding and computation. Nat. Rev. Neurosci. *7*, 358–366.

Bach, M., and Krüger, J. (1986). Correlated neuronal variability in monkey visual cortex revealed by a multi-microelectrode. Exp. Brain Res. *61*, 451–456.

Bair, W., Zohary, E., and Newsome, W.T. (2001). Correlated firing in macaque visual area MT: time scales and relationship to behavior. J. Neurosci. *21*, 1676–1697.

Berens, P., Ecker, A.S., Cotton, R.J., Ma, W.J., Bethge, M., and Tolias, A.S. (2012). A fast and simple population code for orientation in primate V1. J. Neurosci. *32*, 10618–10626.

Blanche, T.J., Spacek, M.A., Hetke, J.F., and Swindale, N.V. (2005). Polytrodes: high-density silicon electrode arrays for large-scale multiunit recording. J. Neurophysiol. *93*, 2987–3000.

Bowdle, T.A., and Ward, R.J. (1989). Induction of anesthesia with small doses of sufentanil or fentanyl: dose versus EEG response, speed of onset, and thiopental requirement. Anesthesiology *70*, 26–30.

Brainard, D.H. (1997). The psychophysics toolbox. Spat. Vis. *10*, 433–436.

Buesing, L., Macke, J., and Sahani, M. (2012). Spectral learning of linear dynamics from generalised-linear observations with application to neural population data, *Volume 25*. (Advances in Neural Information Processing Systems), pp. 1691–1699.

Calabrese, A., and Paninski, L. (2011). Kalman filter mixture model for spike sorting of non-stationary data. J. Neurosci. Methods *196*, 159–169.

Campagna, J.A., Miller, K.W., and Forman, S.A. (2003). Mechanisms of actions of inhaled anesthetics. N. Engl. J. Med. *348*, 2110–2124.

Carandini, M., Heeger, D.J., and Movshon, J.A. (1997). Linearity and normalization in simple cells of the macaque primary visual cortex. J. Neurosci. *17*, 8621–8644.

Chi, O.Z., and Field, C. (1986). Effects of isoflurane on visual evoked potentials in humans. Anesthesiology *65*, 328–330.

Cohen, M.R., and Kohn, A. (2011). Measuring and interpreting neuronal correlations. Nat. Neurosci. *14*, 811–819.

Cohen, M.R., and Maunsell, J.H.R. (2009). Attention improves performance primarily by reducing interneuronal correlations. Nat. Neurosci. *12*, 1594–1600.

Cohen, M.R., and Maunsell, J.H.R. (2010). A neuronal population measure of attention predicts behavioral performance on individual trials. J. Neurosci. *30*, 15241–15253.

Cohen, M.R., and Newsome, W.T. (2008). Context-dependent changes in functional circuitry in visual area MT. Neuron *60*, 162–173.

Constantinople, C.M., and Bruno, R.M. (2011). Effects and mechanisms of wakefulness on local cortical networks. Neuron *69*, 1061–1068.

De Valois, R.L., Albrecht, D.G., and Thorell, L.G. (1982a). Spatial frequency selectivity of cells in macaque visual cortex. Vision Res. *22*, 545–559.

De Valois, R.L., Yund, E.W., and Hepler, N. (1982b). The orientation and direction selectivity of cells in macaque visual cortex. Vision Res. *22*, 531–544.

Denman, D.J., and Contreras, D. (2013). The structure of pairwise correlation in mouse primary visual cortex reveals functional organization in the absence of an orientation map. Cereb. Cortex. http://dx.doi.org/10.1093/cercor/bht128.

Drummond, J.C.M.D. (2000). Monitoring depth of anesthesia: with emphasis on the application of the bispectral index and the middle latency auditory evoked response to the prevention of recall. Anesthesiology *93*, 876–882.

Ecker, A.S., Berens, P., Keliris, G.A., Bethge, M., Logothetis, N.K., and Tolias, A.S. (2010). Decorrelated neuronal firing in cortical microcircuits. Science *327*, 584–587.

Ecker, A.S., Berens, P., Tolias, A.S., and Bethge, M. (2011). The effect of noise correlations in populations of diversely tuned neurons. J. Neurosci. *31*, 14272–14283.

Gawne, T.J., and Richmond, B.J. (1993). How independent are the messages carried by adjacent inferior temporal cortical neurons? J. Neurosci. *13*, 2758–2771.

Gawne, T.J., Kjaer, T.W., Hertz, J.A., and Richmond, B.J. (1996). Adjacent visual cortical complex cells share about 20% of their stimulus-related information. Cereb. Cortex *6*, 482–489.

Goard, M., and Dan, Y. (2009). Basal forebrain activation enhances cortical coding of natural scenes. Nat. Neurosci. *12*, 1444–1449.

Goris, R.L.T., Simoncelli, E.P., and Movshon, J.A. (2013). Response variability of visual cortical neurons explained by a modulated Poisson model. Society for Neuroscience Abstracts.

Gutnisky, D.A., and Dragoi, V. (2008). Adaptive coding of visual information in neural populations. Nature *452*, 220–224.

Haider, B., Häusser, M., and Carandini, M. (2013). Inhibition dominates sensory responses in the awake cortex. Nature *493*, 97–100.

Hansen, B.J., Chelaru, M.I., and Dragoi, V. (2012). Correlated variability in laminar cortical circuits. Neuron *76*, 590–602.

Harris, K.D., and Thiele, A. (2011). Cortical state and attention. Nat. Rev. Neurosci. *12*, 509–523.

Herrero, J.L., Gieselmann, M.A., Sanayei, M., and Thiele, A. (2013). Attention-induced variance and noise correlation reduction in macaque V1 is mediated by NMDA receptors. Neuron *78*, 729–739.

Hubel, D.H., and Wiesel, T.N. (1968). Receptive fields and functional architecture of monkey striate cortex. J. Physiol. *195*, 215–243.

Josić, K., Shea-Brown, E., Doiron, B., and de la Rocha, J. (2009). Stimulus-dependent correlations and population codes. Neural Comput. *21*, 2774–2804.

Kelly, R.C., Smith, M.A., Kass, R.E., and Lee, T.S. (2010). Local field potentials indicate network state and account for neuronal response variability. J. Comput. Neurosci. *29*, 567–579.

Kohn, A., and Smith, M.A. (2005). Stimulus dependence of neuronal correlation in primary visual cortex of the macaque. J. Neurosci. *25*, 3661–3673.

Kohn, A., Zandvakili, A., and Smith, M.A. (2009). Correlations and brain states: from electrophysiology to functional imaging. Curr. Opin. Neurobiol. *19*, 434–438.

Loughnan, B.L., Sebel, P.S., Thomas, D., Rutherfoord, C.F., and Rogers, H. (1987). Evoked potentials following diazepam or fentanyl. Anaesthesia *42*, 195–198.

Macke, J.H., et al. (2011). Empirical models of spiking in neural populations. Adv. Neural Inf. Process. Syst. *24*, 1350–1358.

Mason, A., Nicoll, A., and Stratford, K. (1991). Synaptic transmission between individual pyramidal neurons of the rat visual cortex in vitro. J. Neurosci. *11*, 72–84.

Mitchell, J.F., Sundberg, K.A., and Reynolds, J.H. (2009). Spatial attention decorrelates intrinsic activity fluctuations in macaque area V4. Neuron *63*, 879–888.

Movshon, J.A., Adelson, E.H., Gizzi, M.S., and Newsome, W.T. (1985). The analysis of moving visual patterns. Pontificia Academica Scripta Varia *54*, 117–151.

Movshon, J.A., Albright, T.D., Stoner, G.R., Majaj, N.J., and Smith, M.A. (2003). Cortical responses to visual motion in alert and anesthetized monkeys. Nat. Neurosci. *6*, 3–3, author reply 3–4.

Niell, C.M., and Stryker, M.P. (2010). Modulation of visual responses by behavioral state in mouse visual cortex. Neuron *65*, 472–479.

Nienborg, H., and Cumming, B.G. (2009). Decision-related activity in sensory neurons reflects more than a neuron's causal effect. Nature *459*, 89–92.

Ohiorhenuan, I.E., Mechler, F., Purpura, K.P., Schmid, A.M., Hu, Q., and Victor, J.D. (2010). Sparse coding and high-order correlations in fine-scale cortical networks. Nature *466*, 617–621.

Petersen, C.C.H., Hahn, T.T., Mehta, M., Grinvald, A., and Sakmann, B. (2003). Interaction of sensory responses with spontaneous depolarization in layer 2/3 barrel cortex. Proc. Natl. Acad. Sci. USA *100*, 13638–13643.

Poulet, J.F.A., and Petersen, C.C.H. (2008). Internal brain state regulates membrane potential synchrony in barrel cortex of behaving mice. Nature *454*, 881–885.

Reich, D.S., Mechler, F., and Victor, J.D. (2001). Independent and redundant information in nearby cortical neurons. Science *294*, 2566–2568.

Renart, A., de la Rocha, J., Bartho, P., Hollender, L., Parga, N., Reyes, A., and Harris, K.D. (2010). The asynchronous state in cortical circuits. Science *327*, 587–590.

Schwender, D., Rimkus, T., Haessler, R., Klasing, S., Pöppel, E., and Peter, K. (1993). Effects of increasing doses of alfentanil, fentanyl and morphine on mid-latency auditory evoked potentials. Br. J. Anaesth. *71*, 622–628.

Shadlen, M.N., and Newsome, W.T. (1998). The variable discharge of cortical neurons: implications for connectivity, computation, and information coding. J. Neurosci. *18*, 3870–3896.

Smith, M.A., and Kohn, A. (2008). Spatial and temporal scales of neuronal correlation in primary visual cortex. J. Neurosci. *28*, 12591–12603.

Smith, M.A., and Sommer, M.A. (2013). Spatial and temporal scales of neuronal correlation in visual area V4. J. Neurosci. *33*, 5422–5432.

Smith, M.A., Jia, X., Zandvakili, A., and Kohn, A. (2013). Laminar dependence of neuronal correlations in visual cortex. J. Neurophysiol. *109*, 940–947.

Softky, W.R., and Koch, C. (1993). The highly irregular firing of cortical cells is inconsistent with temporal integration of random EPSPs. J. Neurosci. *13*, 334–350.

Sompolinsky, H., Yoon, H., Kang, K., and Shamir, M. (2001). Population coding in neuronal systems with correlated noise. Phys. Rev. E Stat. Nonlin. Soft Matter Phys. *64*, 051904.

Steriade, M., McCormick, D.A., and Sejnowski, T.J. (1993). Thalamocortical oscillations in the sleeping and aroused brain. Science *262*, 679–685.

Tolias, A.S., Ecker, A.S., Siapas, A.G., Hoenselaar, A., Keliris, G.A., and Logothetis, N.K. (2007). Recording chronically from the same neurons in awake, behaving primates. J. Neurophysiol. *98*, 3780–3790.

Yu, B.M., Cunningham, J.P., Santhanam, G., Ryu, S.I., Shenoy, K.V., and Sahani, M. (2009). Gaussian-process factor analysis for low-dimensional single-trial analysis of neural population activity. J. Neurophysiol. *102*, 614–635.

Zeki, S.M. (1974). Cells responding to changing image size and disparity in the cortex of the rhesus monkey. J. Physiol. *242*, 827–841.

Zohary, E., Shadlen, M.N., and Newsome, W.T. (1994). Correlated neuronal discharge rate and its implications for psychophysical performance. Nature *370*, 140–143.

Neuron, Volume *82*

Supplemental Information

State Dependence of Noise Correlations in Macaque Primary Visual Cortex

Alexander S. Ecker, Philipp Berens, R. James Cotton, Manivannan Subramaniyan, George H. Denfield, Cathryn R. Cadwell, Stelios M. Smirnakis, Matthias Bethge, and Andreas S. Tolias

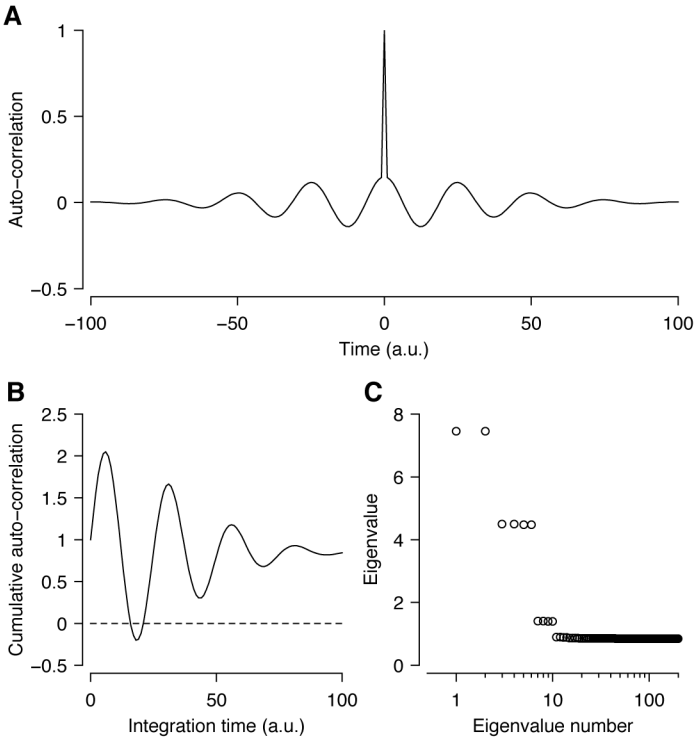

Figure S1. Toy example where the normalization suggested by Bair et al. (2001) fails (related to Fig. 4F). A, Auto-correlation function with oscillatory component. **B,** Cumulative auto-correlation ($A_{jj}(\tau)$, Eq. S2) integrated away from zero as suggested by Bair et al. (2001). Note that the integral becomes negative, leaving $r_{\mathrm{CCG}}(\tau)$ ill-defined for $\tau \approx 20$. **C,** Eigenvalue spectrum of auto-correlation matrix. All eigenvalues are positive, demonstrating that this is an admissible auto-correlation structure.

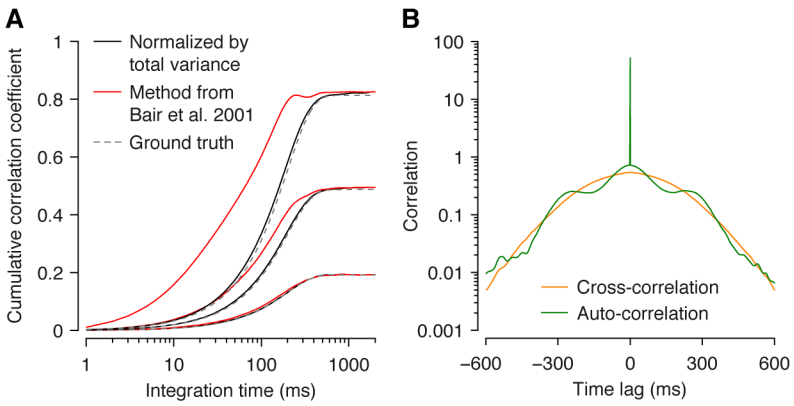

Figure S2. Simulation to illustrate issues with extracting the timescale of correlation by integrating cross-correlogram (related to Fig. 4F). Firing rates were sinusoidally modulated in time (frequency: 3.4 Hz, mimicking simple cell responses to a drifting grating). Correlations were induced by multiplying the firing rate of each neuron by a common, time-varying gain (as in Fig. 6) with auto-correlation timescale of 200 ms (Gaussian kernel, as in Fig. 3A). Spikes were generated as inhomogeneous Poisson processes. **A,** cumulative correlation coefficient, computed by integrating the cross-correlogram and using different normalizations. Red line: normalization from Bair et al. 2001 (Eq. S2). Black line: using our suggested normalization (Eq. S7). Gray dashed line: ground truth (auto-correlation of common gain, rescaled to match in magnitude). **B,** Average shuffle-corrected auto- and cross-correlation functions, $C_{jk}(\tau)$. The stimulus frequency is visible in the auto-correlogram, but not in the average cross-correlogram since we averaged over pairs uniformly covering the full range of preferred phases.

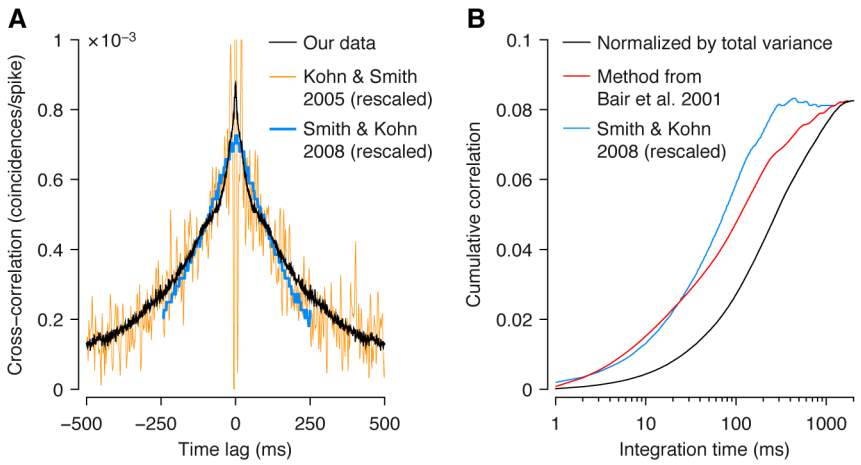

Figure S3. Timescale of correlation extracted from CCG (related to Fig. 4F). A, Average cross-correlation function for pairs recorded by different tetrodes. Black: our anesthetized data; blue: reproduced from Smith & Kohn 2008 (their Fig. 4F, distance: 2 mm) and rescaled to match our level of correlations. Orange: reproduced from Kohn & Smith 2005 (their Fig. 3C, best orientation) and rescaled such that magnitude of the slow component matches our data. **B,** Timescale of correlations extracted by integrating cross-correlogram. Red: r_{CCG} using the original normalization suggested by Bair et al. 2001 (Eq. S2), which underestimates the underlying timescale (see Section 1.2). Blue: same analysis, reproduced from Smith & Kohn 2008 and rescaled such that the total spike count correlation matches our data. Black: r_{CCG} using our suggested normalization (Eq. S7), which yields a less biased estimate of the timescale, more consistent with the parametric estimate obtained from the GPFA model (Fig. 4F).

1 Estimating the timescale of correlations

A previous study in anesthetized monkey V1 (Smith & Kohn 2008) reported that most of the correlations arise on a timescale of less than 100 ms. At first sight this appeared somewhat at odds with our results. Therefore, we investigated the method to identify the timescale of correlations (Bair et al. 2001) used in this study in detail. We found that it leads to a systematic underestimation of the underlying timescale of correlations. In Section 1.2 we explain why this underestimation occurs. We suggest a simple correction to the original definition, which overcomes this problem (Section 1.3). In addition, we compare our data with those of Smith & Kohn 2008 using the same analysis method on both datasets to show that the two datasets are in fact consistent with respect to timescale (Section 1.4).

1.1 Analysis methods: overview

When measuring correlations between neurons, a natural question to ask is what is the timescale of those correlations. The most general approach for addressing this question is to consider the *cross-correlation function* if a time-domain representation is desired or the *cross-spectrum* if a frequency-domain representation is desired. The latter leads to coherence analysis, which provides a frequency-resolved correlation coefficient between two time series (e.g. Brockwell & Davis 2009, p. 436; Box et al. 2008, p. 554). Which method is most appropriate depends on the assumptions about the mechanism generating the correlations and what aspect(s) of the correlation function/cross spectrum one is interested in.

A number of methods have been used in the literature to estimate the timescale of correlations, including integrating the cross-correlogram (e.g. Bair et al. 2001; Smith & Kohn 2008), computing correlations in bins of different sizes (Reich et al. 2001; Hansen et al. 2012), coherence analysis (Mitchell et al. 2009), or parametrically modeling a common input (this study).

1.2 Issues with extracting timescale from cross-correlograms

Bair et al. (2001) suggest a method to extract the timescale of correlations by integrating the cross-correlogram. The reasoning behind this analysis is that if correlations extend only over a finite range of time, the integral will saturate at some point. This point of saturation provides an estimate of the timescale. In addition, when integrating over the full length of a trial, this method is equivalent to computing spike count correlations.

Let $C_{jk}(\tau)$ denote the shuffle-corrected cross-correlation function of neurons j and k (see Bair et al. 2001 for details). We define the cumulative cross-correlation

$$A_{jk}(\tau) = \int_{-\tau}^{\tau} C_{jk}(t)dt. \tag{S1}$$

The cumulative correlation coefficient, r_{CCG}, was originally defined by Bair et al. (2001) as

$$r_{\mathrm{CCG}}(\tau) = \frac{A_{jk}(\tau)}{\sqrt{A_{jj}(\tau)A_{kk}(\tau)}} \tag{S2}$$

While intuitively appealing, this definition is not ideal for several reasons, which are related to the normalization constant in Eq. S2.

First, unlike what one would expect from a correlation coefficient, $r_{\mathrm{CCG}}(\tau)$ is not guaranteed to be between –1 and 1. In fact, it is not even guaranteed to exist, since the cumulative auto-correlation $A_{jj}(\tau)$ can become zero or even negative for perfectly valid auto-correlation functions (Fig. S1). This tends to be the case if there is a strong oscillatory component in the auto-correlation (Fig. S1A).

Second, if a temporally fluctuating common input drives the correlations between two neurons, the definition in Eq. S2 will not recover the underlying temporal structure of this common input, but instead a biased version of it. The magnitude of the bias will increase with the strength of the correlation (Fig. S2A). The reason for this effect can be understood by considering a simple toy example:

$$x_j = z_j + c, \tag{S3}$$

where x_j ($j = 1,2$) is the activity of each neuron, z_j is Gaussian white noise (with unit variance and uncorrelated both in time and across neurons) and c is a slowly fluctuating input common to both neurons with temporal auto-correlation function $K(\tau)$. Under this model, the timescale of the correlation between x_1 and x_2 is identical to the timescale of the fluctuations in c, since it is exclusively the effect of c that generates the correlations. The auto- and cross-correlation functions of $\boldsymbol{x}$ are

$$C_{11}(\tau) = C_{22}(\tau) = K(\tau) + \delta(\tau), \qquad C_{12}(\tau) = K(\tau). \tag{S4}$$

Here, $\delta(\tau) = 1$ if $\tau = 0$ and $\delta(\tau) = 0$ otherwise. We see that the cross-correlation C_{12} is equal to the auto-correlation K of the common input. Consequently, any well-defined measure $\tilde{r}_{\mathrm{CCG}}$ should in this case be proportional to the integral of K:

$$\tilde{r}_{\mathrm{CCG}}(\tau) \propto \int_{-\tau}^{\tau} K(t)dt \tag{S5}$$

However, plugging Eq. S4 into the definition of r_{CCG} above (Eq. S2), we obtain

$$r_{\mathrm{CCG}}(\tau) = \frac{\int_{-\tau}^{\tau} K(t)dt}{1 + \int_{-\tau}^{\tau} K(t)dt} \tag{S6}$$

Since the integral of K enters both the numerator and the denominator, the shape of r_{CCG} does not directly reveal the timescale of the underlying correlations. It is also easy to see from this equation why the bias becomes larger for strong correlations (Fig. S2): while for small correlations the denominator is always close to 1 (and therefore the normalization is approximately correct), for strong correlations the denominator grows at the same speed as the numerator, which in this case leads to an overestimation of the correlations for small τ.

A third, more subtle effect arises when responses are modulated periodically (such as e.g. a simple cell response to a drifting grating) and the common input acts multiplicatively. In this case both cross- and auto-correlograms will contain a periodic component (Fig. S2B). Although the oscillatory component in the cross-correlogram averages out over many neurons that have random phase relations, it remains in the auto-correlogram. This causes the somewhat oscillatory shape in the cumulative correlation when using the normalization in Eq. S2 (Fig. S2A, red line, most evident for strong correlations), which is also visible in both our anesthetized data and that of Smith & Kohn 2008 (Fig. S3B).

1.3 Improved normalization for extracting the timescale

The issues outlined above arise because the normalization depends on τ, which distorts the shape of the cross-correlation function. Since the cross-correlation function already contains all the information about the timescale no normalization is needed to extract it. The main reasons for normalization (in the context of estimating the timescale) are to create the correspondence with spike count correlations when integrating over the entire trial or to ensure that pairs are weighted equally when averaging over many pairs. One possible normalization, which maintains the correspondence with spike count correlations but does not distort the timescale, is the following:

$$r_{\mathrm{CCG}}(\tau) = \frac{A_{jk}(\tau)}{\sqrt{A_{jj}(T)A_{kk}(T)}} \tag{S7}$$

Here, T is chosen such that $A_{jj}(T)$ is an unbiased estimate of the cell's variance. This means that T must be large enough that $A_{jj}(T)$ is saturated, i.e. $\langle A_{jj}(T)\rangle \approx \langle A_{jj}(\infty)\rangle$. The easiest choice is to

use the length of the entire trial. This is what we use for the analysis presented in Fig. S3B below. In this case (and if the correlations do not extend beyond T) $r_{\mathrm{CCG}}(\tau)$ will converge to the spike count correlations for $\tau \to T$. Note, however, that $r_{\mathrm{CCG}}(\tau)$ is not guaranteed to be bounded between -1 and 1 for $\tau < T$. The interpretation as a correlation coefficient thus applies only for large enough τ.

1.4 Timescale of correlations under anesthesia

Smith & Kohn (2008) report that in their anesthetized recordings most of the noise correlations arise on timescales of 100 ms or less (their Fig. 4B), which seems to be somewhat at odds with our findings. However, this apparent discrepancy is not caused by a difference in the data, but instead by the different analysis methods that were used. The shape of the average cross-correlation function in our anesthetized data is very similar to that reported previously under anesthesia (Fig. S3A, Kohn & Smith 2005; Smith & Kohn 2008). In addition, when we used the originally suggested method (Eq. S2; Bair et al. 2001; Smith & Kohn 2008) to analyze our data, we obtained similarly low estimates of the timescale (Fig. S3B, compare the red and blue lines). Given this finding and the general agreement between our anesthetized data and those by Smith & Kohn (2008) we conclude that the two datasets are also fairly consistent with respect to timescale.

Importantly, when we applied the corrected formula (Eq. S7), the results of the cross-correlation analysis were consistent with the parametric approach using the GPFA model (Fig. S3B, black line; Fig. 4F).

2 Supplemental Experimental Procedures

2.1 Surgical procedure in anesthetized monkeys

After premedication with Dexamethasone (0.25–0.5 mg/kg; 48 h, 24 h and on the day of the procedure) and atropine (0.05 mg/kg prior to sedation), animals were sedated with a mixture of ketamine (10 mg/kg) and xylazine (0.5 mg/kg). During the surgery for implanting chamber and tetrode drive anesthesia was maintained using isoflurane (0.5–2%) and fentanyl (7 mg/kg/hr). This surgery was performed in a dedicated operating room under aseptic conditions. A craniotomy was made directly anterior to the occipital ridge approximately 20 mm lateral to the midline, resulting in a recording location over V1 in the lower visual field at eccentricities between 1 and 4 degrees. A cylindrical chamber was positioned around the craniotomy and secured with bone cement. After performing a durotomoy (7 mm diameter) in the center of the craniotomy a bone replacement plate and the tetrode drive were inserted into the chamber and secured with screws. At this point the entire assembly was sealed so there was no risk of infection. After the chamber had been placed the monkeys were transferred to the recording setup, where anesthesia was switched to opioids and the tetrodes were lowered into the brain.

2.2 Data acquisition, spike detection and spike sorting

2.2.1 Data acquisition

For one of the two awake animals spikes were extracted online by threshold crossing and short waveform segments (1 ms, 32 samples) were saved. In addition, local field potentials were acquired continuously at 2 kHz. In the second awake animal, data were acquired continuously at 32 kHz as broadband signal (0.5–16 kHz) using a custom-build system (Ecker et al. 2010). For all three anesthetized animals, data was acquired continuously at 30 kHz as broadband signal (0.3–15 kHz) using a commercially available recording system (Blackrock Microsystems).

2.2.2 Spike detection

Except for one of the awake animals, spikes were detected offline when the signal on any of the four channels crossed a threshold of five times the standard deviation on the corresponding channel. To avoid artificial inflation of the threshold in the presence of a large number of high-amplitude spikes we used a robust estimator of the standard deviation, given by $\sigma = \text{median}(|x|)/0.6745$ (Quiroga et al. 2004). Spikes were aligned to the center of mass of the

continuous waveform segment above half the peak amplitude. Code for spike detection is available online at https://github.com/atlab/spikedetection.

2.2.3 Spike sorting

To extract features for spike sorting, we performed principal component analysis on the extracted waveform segments (individually for each channel). This step reduced the data to three dimensions per channel, resulting in a 12-dimensional feature vector. To deal with potential waveform drift, we use fit mixture model that uses Kalman filters to track changing cluster means over time (Calabrese & Paninski 2011). We model the shape of each cluster by a multivariate *t*-distribution (Shoham et al. 2003) with a ridge-regularized covariance matrix. In our experience, mixture models often use multiple mixture components with similar means to model a single neuron, particularly so for large datasets. Presumably this occurs because clusters tend to have relatively heavy tails (due to spike misalignment and/or overlapping spikes) while the cluster centers are modeled well by Gaussians. Since such clusters have to be grouped manually (which is error-prone) and provide no substantial benefit (the goal is to identify neurons, not to obtain a perfect density model), it is desirable to obtain a model that uses only one mixture component per cluster. We found that this can be accomplished relatively effectively by using *t*-distributions with small degrees of freedom (we use $df = 5$), forcing the algorithm to use a distribution with relatively heavy tails.

The number of clusters was determined based on a penalized average likelihood, where the penalty term was a constant cost per additional cluster. Although this penalty term is a heuristic that requires tuning the cost parameter, we found this approach, in combination with *t*-distributions and regularized covariance estimates (as described above), to result in smaller numbers of clusters and therefore less manual processing than our previous approach based on the Bayesian Information Criterion (BIC). Code for spike sorting is available online at https://github.com/aecker/moksm.

Single unit isolation can be assessed quantitatively using the mixture model. The model provides a posterior distribution over class membership for each spike. From this posterior we estimated the fraction of false positive and false negative assignments for each putative cell. Cells with more than 20% false positives or false negatives as well as those that did not display a clear refractory period were usually grouped into the multi unit cluster during the manual post-processing step and therefore not used for analysis. Since the focus of this paper is on global fluctuations that are distributed among many tetrodes, spike-sorting errors are unlikely

to play an important role since they would affect primarily pairs recorded by the same tetrode (Ecker et al. 2010). Thus, to increase statistical power, we included all units flagged as single units in the analysis. The sum of false positives and false negatives was less than 10% of all spikes for 62% and less than 20% for 83% of all single units in our dataset (awake: 63% and 82%, anesthetized: 61% and 83%).

2.3 Assessment of recording stability

We assessed recording stability by computing the long-term component of the trial-autocorrelogram as described in the main text. The stability criterion was important since the anesthetized experiments were performed acutely and tetrodes were adjusted every 8–10 hours. As a consequence, occasional recording instabilities due to tissue movement were unavoidable. Such instabilities can cause changes in spike amplitudes, which are not a problem (as long as cells remain isolated) since our spike-sorting algorithm can track them. In addition, substantial changes in firing rates can occur, presumably because of loss of isolation, damage to the cell, as a general reaction to the penetrating electrode, or changes in excitability due to physiological reasons. If more than one cell was affected at the same time, the first factor in the GPFA model picked up the instability instead of the global network state. This was easy to detect since in such a case most cells had weights close to zero while only the ones affected by the instability had positive weights and the timescale of the process was very slow. Removing unstable cells solved this problem and resulted in more consistent estimates of weights and timescale. One obvious consequence of this procedure that should be mentioned is that if cells displayed drifts in firing rates over slow timescales due to physiological reasons then our analysis would by definition not recover these slow processes.

2.4 Variance explained and residual correlations in GPFA model

To evaluate the fraction of variance explained (VE; Fig. 3) and the residual correlation structure (Fig. 5) we first fitted the model parameters ($\boldsymbol{c}$, R, and τ) on the training set. We then estimated the network state x on the test set using the E step of the EM algorithm (Yu et al. 2009 Eq. A6). Next, we re-estimated the residual covariance using the M step of the EM algorithm while keeping all other parameters fixed. Here, in contrast to the training set, we did not enforce R to be diagonal but estimated a full covariance matrix, which we denote by Q. Since we worked on the test set the original equations had to be modified (compare to Yu et al. 2009 Eq. A9). We obtained:

$$Q = \frac{1}{T}\sum_{t=1}^{T} \boldsymbol{c}\langle x_t^2\rangle \boldsymbol{c}' - \boldsymbol{c}\langle x_t\rangle \boldsymbol{y}_t' - \boldsymbol{y}_t\langle x_t\rangle \boldsymbol{c}' + \boldsymbol{y}_t \boldsymbol{y}_t' \tag{S8}$$

This matrix can be thought of as the residual covariance matrix after the network state has been accounted for. Variance explained was then computed as

$$\mathrm{VE}_k = 1 - \frac{Q_{kk}}{\mathrm{Var}[y_k]} \tag{S9}$$

where all quantities in Eq. S9 were computed on the test set. This ensured that VE was not over-fitted and was nearly unbiased.

Although we fitted the model on spike counts in 100-ms windows, residual correlations and variance explained can also be evaluated for larger counting windows. Denote by $\boldsymbol{z} = \sum_{t=1}^{T} \boldsymbol{y}_t$ the spike count of an entire trial and define $\tilde{\boldsymbol{c}} = [\boldsymbol{c}, \boldsymbol{c}, \cdots, \boldsymbol{c}]$ (T times). Then we obtain

$$\mathrm{Cov}[\boldsymbol{z}] = \tilde{\boldsymbol{c}} K \tilde{\boldsymbol{c}}' + TR, \tag{S10}$$

and for the residual covariance

$$Q(\boldsymbol{z}) = \tilde{\boldsymbol{c}}\langle \overline{\boldsymbol{x}}\overline{\boldsymbol{x}}'\rangle \tilde{\boldsymbol{c}}' - \tilde{\boldsymbol{c}}\langle \overline{\boldsymbol{x}}\overline{\boldsymbol{x}}'\rangle \boldsymbol{z}' - \mathbf{z}\langle \overline{\boldsymbol{x}}\overline{\boldsymbol{x}}'\rangle \tilde{\boldsymbol{c}}' + \boldsymbol{z}\boldsymbol{z}', \tag{S11}$$

where $\overline{\boldsymbol{x}} = [x_1, \cdots, x_T]'$. Variance explained (Fig. 3) and residual noise correlations (Fig. 5) were calculated for 500 ms windows since this was the maximum available in the awake dataset.

Supplemental references

Box, G.E.P., Jenkins, G.M. & Reinsel, G.C., 2008. *Time Series Analysis: Forecasting and Control* 4th ed., Wiley.

Brockwell, P.J. & Davis, R.A., 2009. *Time Series: Theory and Methods* 2nd ed. 1991. 2nd printing., Springer, Berlin.

Quiroga, R.Q., Nadasdy, Z. & Ben-Shaul, Y., 2004. Unsupervised Spike Detection and Sorting with Wavelets and Superparamagnetic Clustering. *Neural Computation*, 16(8), pp.1661–1687.

Shoham, S., Fellows, M.R. & Normann, R.A., 2003. Robust, automatic spike sorting using mixtures of multivariate t-distributions. *Journal of Neuroscience Methods*, 127(2), pp.111–122.